The Thesis Committee for Jeffrey Robert Sitgreaves
Certifies that this is the approved version of the following thesis:

Shelf-to-Basin Architecture and Facies Variability of a Cretaceous Intrashelf Basin in the Northwest Gulf of Mexico

APPROVED BY
SUPERVISING COMMITTEE:

Supervisor:

Charles Kerans

Robert G. Loucks

William L. Fisher

Shelf-to-Basin Architecture and Facies Variability of a Cretaceous Intrashelf Basin in the Northwest Gulf of Mexico

by

Jeffrey Robert Sitgreaves, B.S.

Thesis

Presented to the Faculty of the Graduate School of

The University of Texas at Austin

in Partial Fulfillment

of the Requirements

for the Degree of

Master of Science in Geological Sciences

The University of Texas at Austin

December, 2015

Dedication

To Andy and Kay for your guidance, love, and encouragement

To Elena, your unconditional love and support made this possible

Acknowledgements

It is often said that the graduate experience depends upon the relationship between the student and advisor. I am thankful to have an advisor that I regard as a tremendous geologist, and as a close friend. Thank you Dr. Charles Kerans for seeing my potential and for always motivating me to achieve that. Your support, advice, and encouragement have helped make me into a better geologist, and made this research possible. I look forward to continuing our work together in the future.

This thesis benefited from the guidance of committee members Dr. Robert Loucks and Dr. William Fisher, their valuable feedback and comments helped significantly improve this manuscript. I gratefully acknowledge the research scientist and staff of the Reservoir Characterization Research Laboratory (RCRL) and the Bureau of Economic Geology (BEG) that helped make this research possible: Dr. Christopher Zahm, Dr. Xavier Janson, Josh Lambert, Stephaine Lane, and Dallas Dunlap. I am also thankful to my fellow graduate students in the RCRL. The late nights and long hours were enjoyable because of our close friendship. I value and cherish the memories we have made together on all of our adventures. I would particularly like to thank Ben Smith and Kris Voorhees, for the late night brainstorms, review of this thesis, and for assistance during fieldwork.

Finally, I would like to thank my family for their unwavering support and encouragement throughout this process. I am blessed to have grown up as part of a supportive and caring family. My parent's guidance and examples have made me into the person I am today. To my fiancé Elena, your love and support made this process possible. You are my foundation; you keep me grounded while always pushing me to become a better man. I am excited to start the next chapter of our lives together.

Abstract

Shelf-to-Basin Architecture and Facies Variability of a Cretaceous Intrashelf Basin in the Northwest Gulf of Mexico

Jeffrey Robert Sitgreaves, M.S Geo. Sci.

The University of Texas at Austin, 2015

Supervisor: Charles Kerans

The geomorphic expression of intrashelf basin systems (ISBs) and their associated facies patterns is extremely subtle, with shelf-to-basin dip angles that can average 0.3° across the slope profile. This presents an issue to stratigraphers working to understand facies variability at the reservoir-scale because the changes in stratal geometries at the shelf-to-basin transition will occur beneath the resolution of conventional subsurface datasets. Exposures along the Pecos River Canyon provide a unique opportunity to observe the transition from grain-dominated facies of the ramp crest into planktonic foraminifera mudstones/wackestones of the intrashelf basin.

For this study, 475 m of detailed sections were collected at five localities and integrated with a high-resolution 3D digital outcrop model (DOM) to document the relationship between vertical facies successions and stratal geometries of the intrashelf basin profile. The high-resolution DOM provides the ability to accurately interpret the subtle depositional dips of the shelf-to-ISB profile that range from less than 0.1° to 0.7°.

The development of the differential topography and facies changes associated with the formation of the Maverick ISB is attributed to differential sediment accumulation rates between active rudist-skeletal shoal formation versus deeper-water foraminiferal mudstones of the basin-center. Rudist bank deposition early in the Albian 6 Composite Sequence formed the positive topographic relief (1-3m) that led to the localization of rapid shallow-water sediment accumulation. After the development of subtle topographic expression, ensuing changes in relative sea-level promoted the development of ISB margins that were dominated by rudist faunal assemblages. The development of the ISB margin increasingly led to the differentiation between the grain-dominated facies along the margin and deposition of globigerinid mudstones in the basin-center.

The extensive and largely undeformed exposures along the lower Pecos River Canyon and adjacent Amistad Reservoir provide clear evidence of the constructional differential-accumulation-driven formation for the Maverick ISB. Similar constructional models are likely for the East Texas and Fort Stockton ISBs on the Texas Comanche Shelf. Similar constructional progressions have been called on for the Bab intrashelf basin and the Natih-E Formation in the Cretaceous of the Middle East.

Table of Contents

List of Figures

SUPPORT AND ORGANIZATION

The financial support for this work was provided by the Reservoir Characterization Research Laboratory at the Bureau of Economic Geology. The participation of industry sponsors in the research of the RCRL allowed for financial support and encouragement of this study. This work also received financial support from the Jackson School of Geosciences at The University of Texas at Austin. This study utilized a number of commercial software and benefited from support in the form of academic licenses provided by Agisoft and Applied Imagery. Additionally, DecisionSpace® was used to construct the stratigraphic framework for the Maverick Intrashelf Basin and the authors are grateful to Halliburton for providing the software and training. Finally, we are thankful for the help of Gregg Gibbs and the Pecos River Ranch for providing us with land access to the Lower Pecos River.

The present study is formatted into a single chapter with a number of sub-sections focusing on the geomorphic expression and facies patterns across the subtle shelf-to-intrashlef basin transition of the Late Albian Maverick Intrashelf Basin in the Northwest Gulf of Mexico. New methods in digital outcrop modeling were utilized in this study to document the 15 km shelf-to-ISB transition at a resolution/cost previously unmatched. A key component of this study was to provide evidence of the constructional differential-accumulation-driven formation of the Maverick ISB. The continuous exposures along the Lower Pecos River provide one of the only outcrop analogs where it is possible to document this transition between the shelf and intrashelf basin.

The work presented in this chapter has been prepared for submission to the Gulf Coast Association of Geological Societies (GCAGS) Journal.

CHAPTER 1: SHELF-TO-BASIN ARCHITECTURE AND FACIES VARIABILITY OF A CRETACEOUS INTRASHELF BASIN

ABSTRACT

The geomorphic expression of intrashelf basin systems (ISBs) and their associated facies patterns is extremely subtle, with shelf-to-basin dip angles that can average 0.3° across the slope profile. This presents an issue to stratigraphers working to understand facies variability at the reservoir-scale because the changes in stratal geometries at the shelf-to-basin transition will occur beneath the resolution of conventional subsurface datasets. In order to address this issue, outcrops that capture the shelf-to-basin transition from the late Albian (Cretaceous) Maverick Intrashelf Basin were mapped along a 15 km dip-oriented transect on the lower Pecos River. This study takes a quantitative approach to characterize the relationships between dip angles, paleo-bathymetry, and sediment production along the shelf-to-ISB profile. This research provides detailed documentation of an intrashelf basin that can function as an outcrop analog for fields producing from similar reservoir settings by improving the understanding of facies variability away from the wellbore.

Exposures along the Pecos River Canyon provide a unique opportunity to observe the transition from grain-dominated facies of the ramp crest into planktonic foraminifera mudstones/wackestones of the intrashelf basin. For this study, 475 m of detailed sections were collected at five localities and integrated with a high-resolution 3D digital outcrop model (DOM) to document the relationship between vertical facies successions and stratal geometries of the intrashelf basin profile. Over 800 photographs were captured and located using Differential Global Navigation Satellite System (GNSS) methods to model the vertical canyon walls that vary in height from 90-115m across the 15km transect. The high-

resolution DOM provides the ability to accurately interpret the subtle depositional dips of the shelf-to-ISB profile that range from less than 0.1° to 0.7°.

The development of the differential topography and facies changes associated with the formation of the Maverick ISB is attributed to differential sediment accumulation rates between active rudist-skeletal shoal formation versus deeper-water foraminiferal mudstones of the basin-center. Rudist bank deposition early in the Albian 6 Composite Sequence formed the positive topographic relief (1-3m) that led to the localization of rapid shallow-water sediment accumulation. After the development of subtle topographic expression, ensuing changes in relative sea-level promoted the development of ISB margins that were dominated by rudist faunal assemblages. Shallow-water basin margins consist of either lagoon-inlet-barrier or foreshore-shoreface grainstones with upper shoreface-foreshore sub-environments demonstrating that the platform built to sea-level. Within the same stratigraphic interval, skeletal wackestones and globigerinid mudstones are deposited in an intrashelf basin setting. The location of a paleo-shoreline and intrashelf basins facies within the same high-frequency sequence allows for the estimation that the total shelf-to-basin relief of the Maverick ISB was greater than 50 meters. The forced regressive highstand deposits of the Albian 21 HFS form the final phase of high-progradation-rate basin filling. These prograding shoreface deposits downlap the condensed mud-rich intrashelf basin facies of the Albian 19 and 20 HFS, and infill the topography formed by the differential aggradation of the intrashelf basin margins.

The extensive and largely undeformed exposures along the lower Pecos River Canyon and adjacent Amistad Reservoir provide clear evidence of the constructional differential-accumulation-driven formation for the Maverick ISB. Similar constructional models are likely for the East Texas and Fort Stockton ISBs on the Texas Comanche Shelf.

Similar constructional progressions have been called on for the Bab intrashelf basin and the Natih-E Formation in the Cretaceous of the Middle East.

INTRODUCTION

Intrashelf basins are unique carbonate depositional system that are characteristic of greenhouse platforms. The development of intrashelf basin systems (ISBs) occurs on the shelf-top, protected behind the shallow rim of a carbonate platform (Read, 1985, 1998). ISBs are geologically short-lived basins that are shallow features (50-150m water depth), that reach several hundred kilometers across (Burchette and Wright, 1992). The formation of ISB depositional systems creates some of the most prolific hydrocarbon systems in the world (e.g, Jurassic-Cretaceous of the Arabian Plate). ISBs are often efficient and self-contained petroleum systems where significant accumulations of organic-rich mudrocks occurs on the broad shelf top, immediately adjacent to potentially high-quality carbonate reservoir facies (Murris, 1984; Van Buchem et al., 2002b; Ziegler, 2001). The occurrence of intrashelf basins is common throughout greenhouse periods of the geologic record. Early examination of intrashelf basins were conducted in the Cambrian Nolichucky Formation by Markello and Read (1981) and the Jurassic Abenaki Formation documented by Eliuk (1978). The most investigated ISBs are located on the Arabian Plate, studies include the Jurassic Hanifa Formation (Droste, 1990; Murris, 1984; Ziegler, 2001), the Aptian Bab ISB (Alsharhan, 1985; Van Buchem et al., 2002a) and the Cenomanian Mishrif-Savark-Natih Formation (Burchette, 1993; Droste and Van Steenwinkel, 2004; Razin et al., 2010; Van Buchem et al., 2002b). Several ISBs have also been identified on the Cretaceous Comanche Platform in the Northwest Gulf of Mexico, including the Maverick ISB (Kerans et al., 1995; Rose, 1974), and the Fort Stockton ISB (Zahm, 1997). Most recently, Bourget et al. (2013) has proposed evidence for the Quaternary Maltia Intrashelf Basin in NW Australia, which would be the first documented example of a Cenozoic ISB.

Intrashelf basins typically have an origin that is constructional, meaning that basin formation is driven by differential sedimentation rates that develop across the carbonate factory, while receiving little input from tectonics or compaction. The constructional development of intrashelf basins raises several questions about the main drivers behind the origin and the specific controls driving the differential sedimentation rates that influence the evolution of these systems (Van Buchem et al., 2002b). In particular, what is the ability of the carbonate factory to develop a topographic response to eustatic fluctuations and ecoeustatic drivers? How can relatively subtle topographic expression lead to the complete shut-down of carbonate productivity in the basin-center? What factors influence the deposition and preservation of organic-rich source rocks within intrashelf basins?

This study provides detailed documentation of the shelf-to-basin evolution of the Late Albian Maverick Intrashelf Basin across four high-frequency sequences that record the changing profile. Quantifying the change in stratal geometries and component facies allows for improved understanding of the dynamic ISBs profile. The shelf-to-basin transition is marked by a gradually changing depositional profile and associated lateral shifts in carbonate skeletal grainstone and mudstone deposits. The exposures along the lower 15km of the Pecos River in western Val Verde County (Fig. 1) provide evidence of low-angle (0.3 degrees) clinoforms and downlap of grainstones onto basin-centered mudstones of the Maverick ISB. The Pecos River Canyon is ideal for this investigation because (1) it offers one of the only opportunities to trace the shelf-to-basin transition of a carbonate ramp depositional system from the inner ramp into intrashelf basin deposits, (2) it provides continuous exposures with manageable accessibility, (3) the outcrop-scale is on the order of subsurface reservoirs (50km of near-continuous dip profile), and (4) has the ability to serve as an analog for reservoirs producing from rudist margins surround mudstone deposits on the shelf-top.

Outcrop analog modeling for reservoir characterization is an important research approach that can provide insight in stratal geometric relationships in subsurface reservoirs that can be difficult to recognize with typical subsurface data (Kerans et al., 1994). The motivation behind the development of outcrop analogs is to build an understanding of the depositional system and facies patterns at the interwell scale to help reduce uncertainty for reservoir modeling in carbonate environments (Howell et al., 2014; Kerans and Tinker, 1997). The Late Albian Maverick Intrashelf Basin outcrop analog can be compared with reservoirs that produce from similar rudist-bearing facies that rim the Aptian Bab Intrashelf Basin (e.g, Bu Hasa fields and Al Huwaisah; (Van Buchem et al., 2002a; Yose et al., 2006)), and has similarities with ISB development in the Cenomanian Natih Formation (Alsharhan, 1995; Van Buchem et al., 2002b). The outcrop study of the Maverick ISB will provide documentation of the changes in depositional facies that are linked to changing stratal geometries at the high-frequency-sequence scale. This facies-stratal geometry link will improve our ability to predict the distribution of high-energy grain-dominated facies and their mud-dominated ISB counterparts in the subsurface.

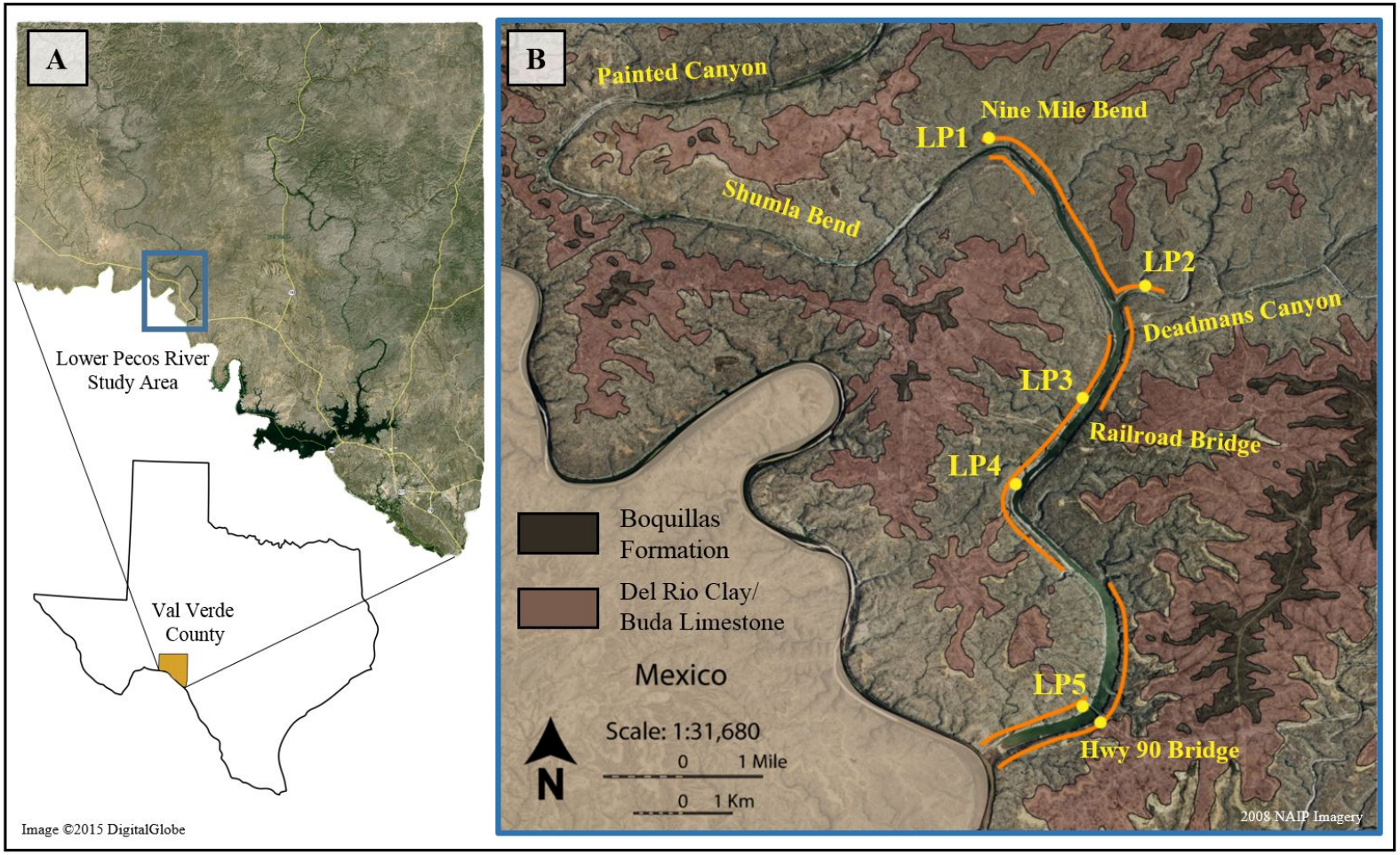

Figure 1: Location of the Lower Pecos River Canyon in Val Verde County, Texas. Interpretation of the Del Rio Clay and Boquillas Formation on 30 cm resolution NAIP Aerial Imagery. Included on the base map are the location of key landmarks (yellow text), the five measured sections (yellow dots), and digital outcrop models (orange lines).

GEOLOGIC AND STRATIGRAPHIC SETTING

The exposures of the Late Albian Maverick ISB are situated on the Comanche Shelf, protected behind the Stuart City Reef Trend that rimmed the ancestral Gulf of Mexico (Bebout and Loucks, 1974; Lehmann et al., 1998; Rose, 1974; Wilson, 1975; Winker and Buffler, 1988). The presence of localized Salmon Peak type facies (skeletal wackestones/mudstones) behind the Stuart City Reef Trend occurs frequently across the continuous Albian (Cretaceous) shelf that spanned from Mexico to Florida (Salvador, 1991; Winker and Buffler, 1988). Across Texas, there were three active intrashelf basin depositional systems during the Early Cretaceous: the Maverick ISB, Fort Stockton ISB, and the East Texas ISB (Fig. 2). These three ISBs highlight two very distinct styles of intrashelf basin origin and duration. The Maverick ISB and the Fort Stockton ISB were geologically short-lived basins that evolved as a result of differential sediment accumulation rates, meaning sedimentation along the ramp margin was greater than sedimentation in the basin, creating differential topography. During the late Albian, the East Texas Basin (ETXB) is also considered an ISB because there is globigerinid mudstone accumulation behind the Stuart City Margin. The origin of the ETXB contrasts significantly to the Maverick and Fort Stockton ISB origin. The ETXB formed as the result of a failed rift in the Jurassic that occurred north of the principle rift that formed the Gulf of Mexico (Jackson and Seni, 1983). Other major structural elements that influence sedimentation in the Northwest GOM are a series of uplifts and tectonic lows; Llano Uplift, Sabine Arch, Coahuilla Platform, San Marcos Arch, and the Sabinas Basin (Salvador, 1991). Sediment distribution across the late Albian Comanche Shelf is highlighted by the distribution of shallow platform sediments, grain-dominated rudist margins, and mud-dominated intrashelf basin deposits with respect to the preexisting reef tend of Stuart City

shelf margin that separates the shelf from the ancestral GOM. (Fig. 2) (Lehmann et al., 2000; Osleger et al., 2004; Rose, 1974; Smith et al., 2000; Winker and Buffler, 1988)

Regional Stratigraphy

In the Northwestern Gulf of Mexico, the first-order tectono-eustatic rise is characterized by the transition from evaporite and clastic-dominated facies assemblages in the Jurassic to carbonate-dominated facies throughout the Cretaceous (Bebout and Loucks, 1974). There are four Cretaceous Supersequences (K1-K4) identified in the Northwest GOM (Goldhammer, 1991; Goldhammer and Johnson, 1999). Within these four supersequences, Phelps et al. (2014) identified seven composite sequences from the Hauterivian through the early Campanian that frame the shelf architecture of the Comanche Platform along the San Marcos Arch. Deposition within the Albian can be further divided into six shorter-duration composite sequences capturing the final stage of Albian deposition and the outcrops along the Pecos River. The youngest Albian composite sequence is composed of six high-frequency sequences (HFS) (Fig. 3) (Kerans et al., 1995). The Albian 18-21 HFS comprise the Albian 6 Composite Sequence, which characterize deposition of the final highstand episode of the K2 Supersequence. The final stage of deposition of the Maverick ISB is marked by the backstepping Albian 22 and 23 HFS, and compose the initial transgressive deposits within the K3 Supersequence.

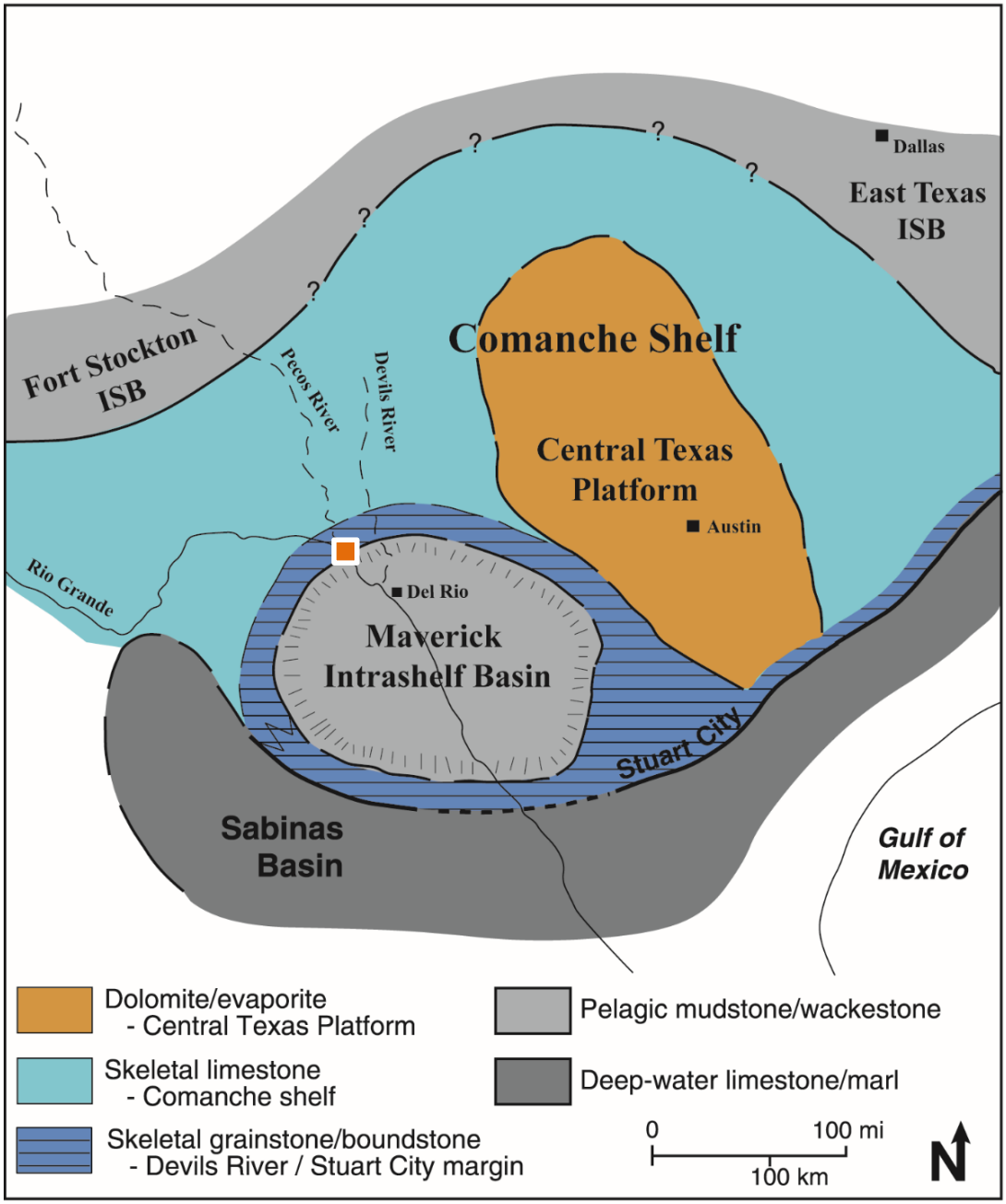

Figure 2: Paleogeographic Map for the Late Albian of the Comanche Shelf in the NW Gulf of Mexico. Note the location of three Intrashelf Basins on the shelf-top; Maverick ISB, Fort Stockton ISB, and the East Texas ISB. Study location is highlighted by the orange square along the northern margin of the Maverick ISB. Modified after Osleger, (2004), Rose, (1974), Smith (2000), and Winker and Buffler, (1988).

The Albian 6 Composite Sequence

At the end of Fredericksburg time (Al5 CS; Al17 HFS) there was a stage of progradation that led to the formation of a fully-aggraded flat-topped platform. Evidence for complete basin aggradation is highlighted by the deposition of tidal flat and evaporite facies of the Fredricksburg-Fort Terret Formation over areas that were previously the Maverick Basin during Glenn Rose (early Albian) time (Kerans et al., 1995; Lehmann et al., 1998). The next major stage of development is a transgression that caused rudist buildup assemblages formerly centered around the Stuart City Margin to backstep nearly 150 km landward of the margin onto the Devil's River uplift (Kerans, 2002; Lehmann et al., 1998; Webster, 1980; Winker and Buffler, 1988). The backstep of rudist buildups formed the margins of the northern Maverick ISB, which is loosely defined in early studies by the Devils River trend (Lozo and Smith, 1964). During this major transgression, there was focused sediment accumulation, local aggradation, and progradation that created margins with positive topographic relief. These margins surrounded a broad area of greater bathymetry and slower rates of sedimentation that define the Maverick Intrashelf Basin. After the establishment of the ramp margin around the Maverick ISB there was a final period of progradation with a seaward-step of grainstones more than 30 km. This episode of progradation is documented along the northern and western margins of the Late Albian Maverick Intrashelf Basin (Kerans et al., 1995; Osleger et al., 2004).

One of the earliest investigations of the Devils River–Salmon Peak Formations along the Lower Pecos River was by Lozo and Smith (1964) to refine the lithostratigraphic terminology. Other studies have made observations of lateral facies relationships and environmental interpretations across much of the Comanche Platform (Rose, 1974; Smith, 1981; Smith et al., 2000). Based on an extensive field investigation along the Pecos River, Kerans et al. (1995) defined the high-resolution sequence stratigraphic framework for the

Late Albian Maverick Intrashelf Basin by tracing HFS boundaries across nearly 50 km of dip-oriented exposures. The established sequence stratigraphic framework consists of the six high-frequency sequences (Albian 18-23 HFS), and covers depositional environments of the ramp system that range from peritidal inner ramp to intrashelf basin (Fig. 3). The first four HFS represent deposition of the Albain 6 CS and sedimentation in the Albian is completed with the backstepping sequences of the Albian 22 and 23 HFS. The Albian 18-23 HFS (Devils River-Salmon Peak Formations) are overlain unconfromably by the Del Rio Clay and Buda Limestone. The lithostratigraphic terminology developed by Lozo and Smith (1964) that was later revised by Rose (1974) can be compared and placed into the sequence stratigraphic framework constructed by Kerans et al. (1995) (Fig. 4).

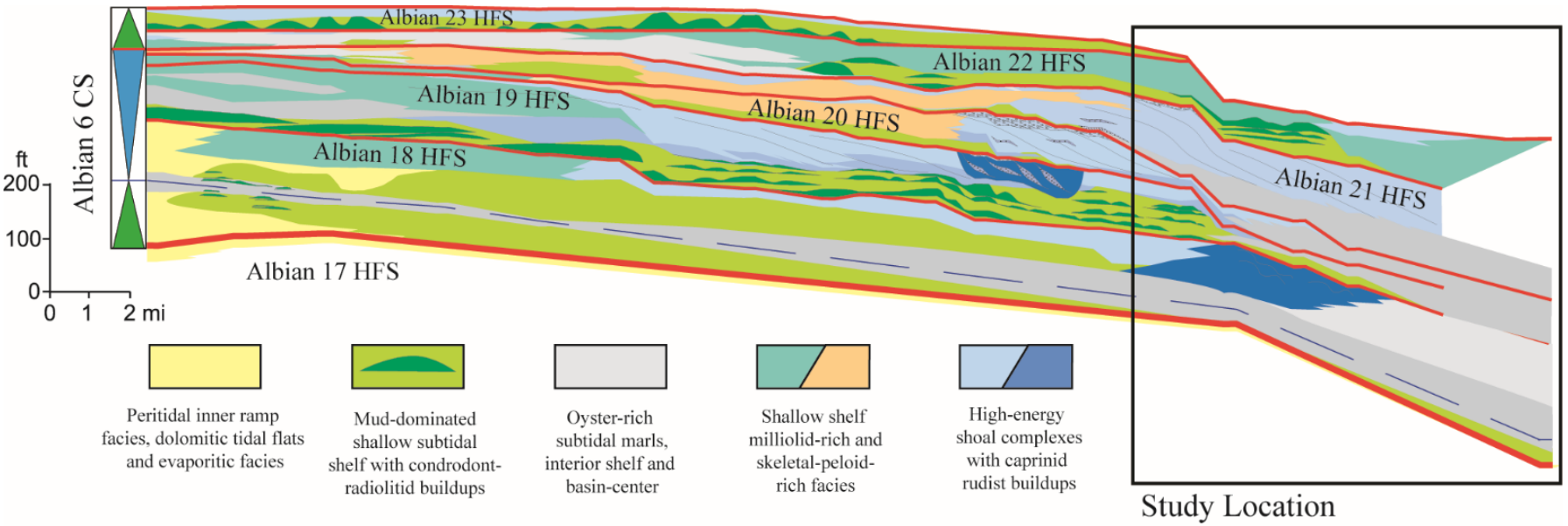

Figure 3: Late Albian high-resolution sequence stratigraphic framework showing the six high-frequency sequences, and the relationship between facies tract and systems tracts. The focus for this study along the lower Pecos River are indicated by the orange box. Modified from Kerans, 2002.

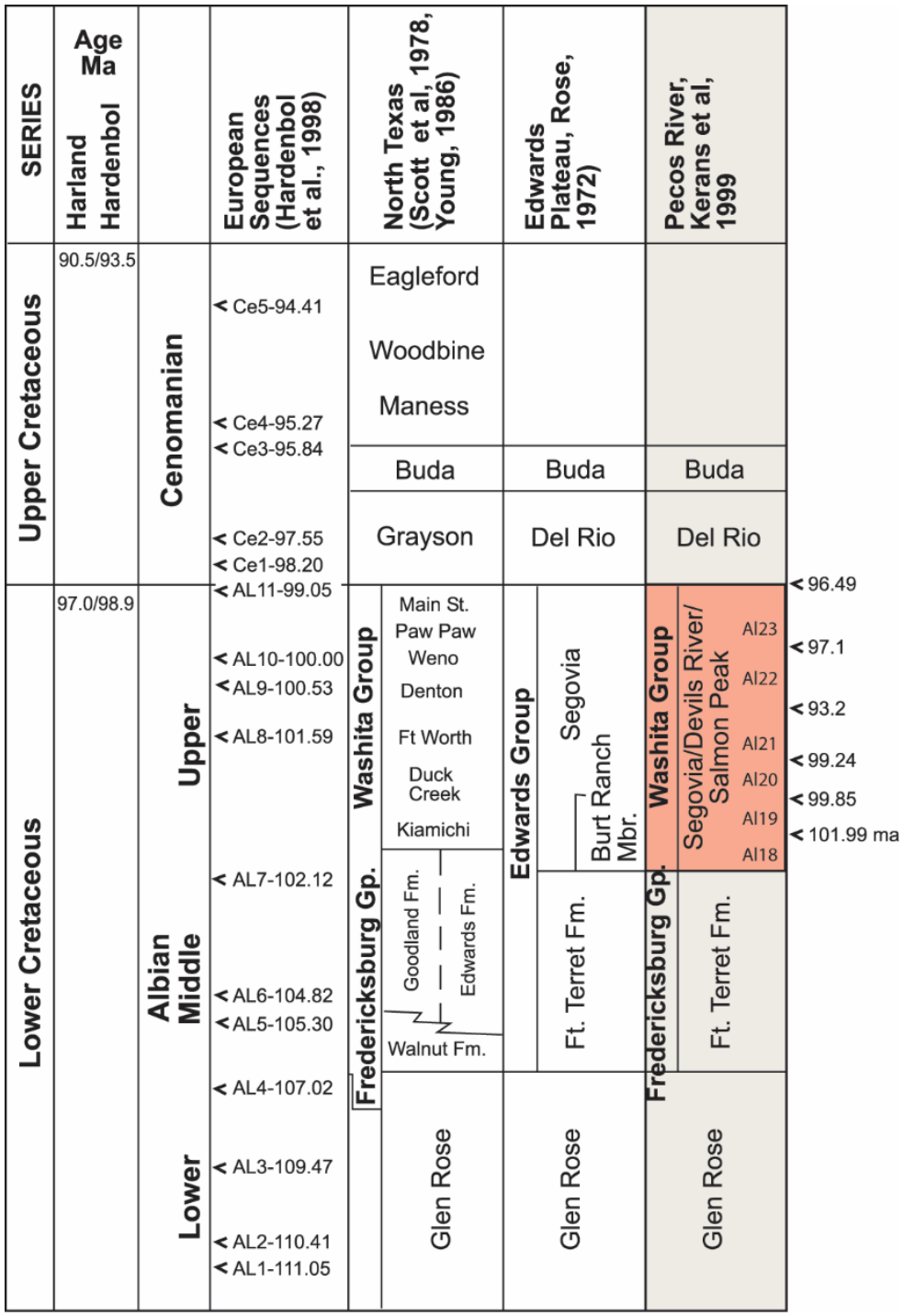

Figure 4: Stratigraphic Column of the Pecos River showing the relationship to lithostratigraphic terminology and highlighting key age constraints for the six Albian high-frequency sequences. The area of focus for this study is mark in red. Modified after Kerans, 2002 and Scott and Kerans, 2002.

DATA AND METHODS

The methodology used for this study includes 1) standard field-based outcrop mapping and collection of measured sections 2) acquisition of ground-based GNSS-calibrated photographs used for the construction of a digital outcrop model using the latest photogrammetry techniques (commercial software: Agisoft) 3) Integration of vertical sections with the dense point clouds to map key HFS boundaries (commercial software: QT Modeler) and 4) stratigraphic modeling using a refinement gridding process combined with set conformance rules and modeled within a stratigraphic framework package (commercial software: Landmark DecisionSpace). Examples of the acquisition, processing, interpretation and modeling stages of this study are provided in Figure 5.

Outcrop-based Sections-Facies Characterization

A total of 475 meters of measured sections were collected across five locations along a dip transect at an average spacing of 1.5 km on the Lower Pecos River Canyon (LPR1-LPR5) (Fig. 1). Sections were logged at a 20 cm resolution following the correlation and stratigraphic analysis methods outlined in detail by Kerans and Tinker (1997). Additionally, 110 hand samples and a series of outcrop photographs were collected to verify the field descriptions of lithofacies (using the Dunham Classification; Duhnam, 1962; Lucia, 1995), weathering, sedimentary structures, and bedding characteristics. From the collected hand samples, 25 thin sections were taken along a vertical transect of the LPR4 measured section to provide petrographic documentation of facies including the important condensed intrashelf basin facies within the Albian 19 and 20 HFS.

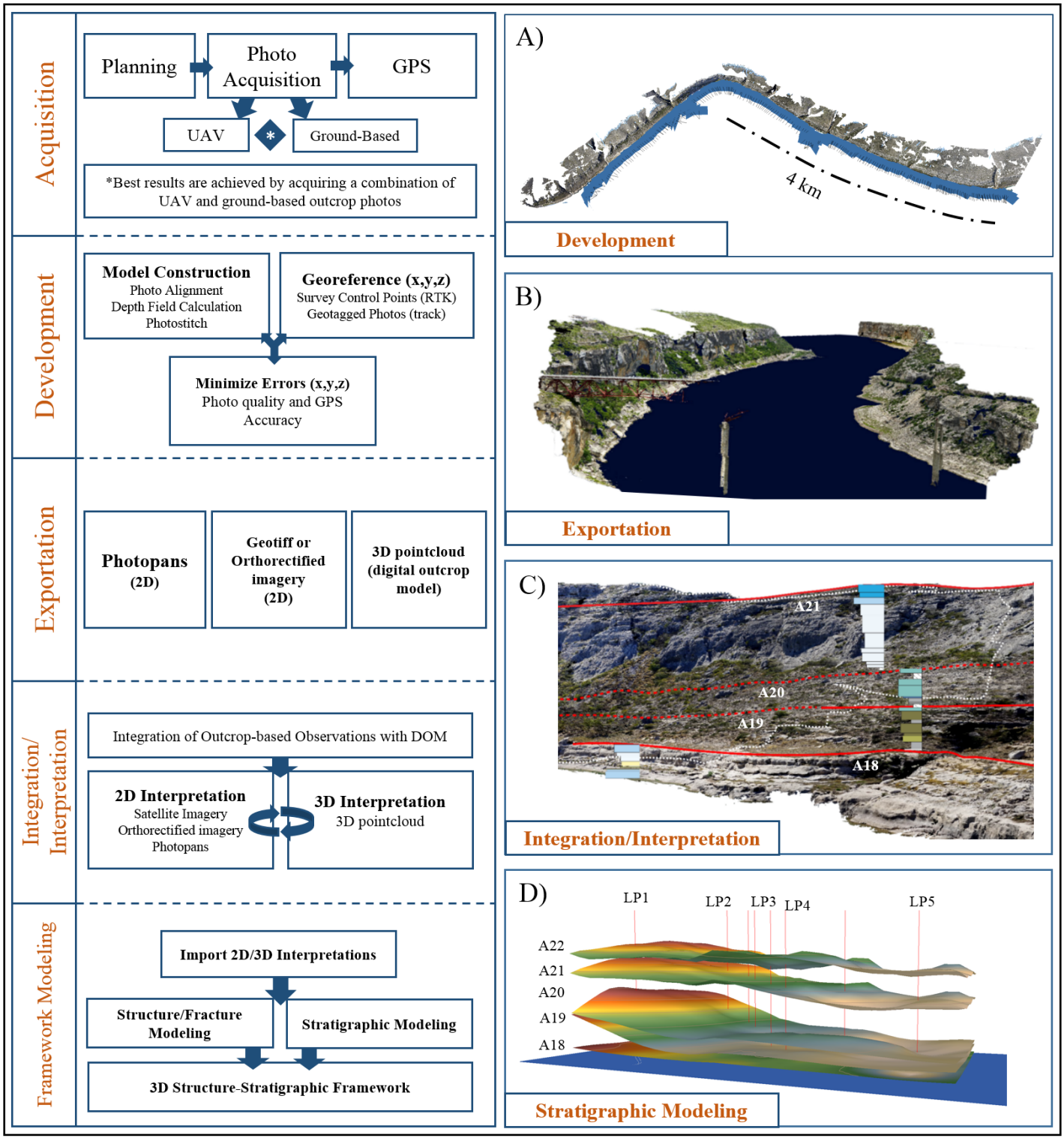

Figure 5: Digital outcrop modeling workflow and examples. Continued on next page.

Figure 5, cont. Successful construction of a digital outcrop model begins with the proper acquisition plan followed by a comprehensive development process. The exportation and interpretation on 3D pointclouds presents the opportunity to model outcrop-mapped surfaces into a high-resolution 3D framework. Method examples: A) Development of a digital outcrop model using photogrammetry. 250 photographs were used to create a dense pointcloud with over 400,000,000 points. B) 3D dense pointcloud at the Highway 90 Bridge with 2 cm/pixel resolution C) Integration of the LP4 measured section with the pointcloud that guided the interpretation of the HFS boundaries D) Stratigraphic framework using interpretations from the digital outcrop model and 5 measured sections. Modified after Zahm and Kerans, 2014.

This research builds upon the sequence stratigraphic framework that was established by Kerans et al. (1995) and modified later in Kerans (2002), in a study that collected a series of 35 measured sections across 50km dip-oriented transect of the Pecos River. The sequence stratigraphic principles of this study follow models initially developed for siliciclastic sequences by Mitchum and Van Wagoner, (1991); Vail, (1987); Van Wagoner et al., (1990) and further modified for applications in carbonates environments by Handford and Loucks, (1993); Kerans and Tinker, (1997). The sequence hierarchy and carbonate ramp environment terminologies will follow those established by Burchette and Wright (1992) and modified by Kerans and Fitchen (1995) with detailed outcrop study on the sequence architecture of the San Andres Formation.

Three-dimensional Digital Outcrop Modeling - Photogrammetry

The evolution of digital outcrop modeling techniques has been fueled by the need to process large field-scale datasets, allow for advanced visualization, and provide the ability to quantify depositional geometries and geobodies that can serve as analog inputs into subsurface reservoir models. Perhaps the most revolutionary advance in digital outcrop modeling was the development and application of LiDAR for use in outcrop characterization by Bellian et al. (2005). Pringle et al. (2006) conducted a review on a variety of methods (including LiDAR and photogrammetry) for digital outcrop modeling and for studying outcrop analogs. Early work with photogrammetry used a small number of aerial photographs to create georegistered orthophotomosaics and low-resolution Digital Surface Models (4m resolution) (Pringle et al., 2004). Modern photogrammetry methods use a series of overlapping photographs taken at a variety of different angles, with given camera orientations/locations to create high-resolution 3D point clouds. In the last few years, there has been significant improvements in terrestrial photogrammetry methods that

allow for digital outcrop model (DOM) construction that is comparable with LiDAR accuracies, and have clear advantages over LiDAR with significant decreases in cost and acquisition time as well as automatic integration of RGB data to the point cloud (Strecha et al., 2015). Recent advances in photogrammetry combined with the advantage of aerial perspectives obtained from Unmanned Aerial Vehicles is becoming the standard for outcrop characterization. Major outcrop characterizations efforts are currently applying UAV technologies with photogrammetry methods to conduct high-resolution facies and fracture mapping at unprecedented scales (Zahm and Kerans, 2014).

Over 800 outcrop photographs were collected for the construction of high-resolution digital outcrop models on the Lower Pecos River. GNSS tracks were collected with a backpack mounted Trimble Pro 6H Receiver and post-processed Differential GNSS was used to get sub-meter horizontal and vertical accuracies. The photographs were captured using a Sony A7R (36mp) camera with a Cannon EF 24-105mm lens mounted to a monopod. Camera locations were obtained by synchronizing the timestamps of the DGNSS tracts with the camera, and then correcting for the offset between the receiver and camera position. The integration of location with the outcrop photographs significantly decreases field acquisition time by several hours and processing time by days. Three-dimensional outcrop models were constructed using Agisoft Photoscan® software on a workstation. The DOM construction process is computer intensive with typical model run times that take over 30 hours to complete despite a robust CPU/RAM workstation configuration. Resolutions obtained by using terrestrial based photogrammetry methods on the Lower Pecos River were at 2 cm/pixel with a 1.5m average camera location error (x,y,z).

Interpretation and Stratigraphic Modeling

The interpretation of a high-density point clouds requires specialized software that is designed to handle high-resolution datasets (model sizes are roughly equivalent to a field-scale 3D seismic survey). With the rapid innovation of acquisition and processing technologies, the next area for advancement will focus on the interpretation and application of these 3D datasets to subsurface analogs. Current research efforts are applying innovative interpretation and quantification techniques on (UAV-based DOM) datasets collected in carbonate settings to help build an understanding of complex facies architectures and fracture patterns (e.g., Zahm and Kerans, 2014).

This outcrop investigation, focused on the interpretation of the Albian 18-22 high-frequency sequences along the lower Pecos River Canyon. The interpretations were made based on field-based tracing of the sequence boundaries and integrating these with vertical measured sections. The interpretations were then made on the 3D DOM across a 9km segment of the lower Pecos River. These interpretations were then exported from a visualization based software and into Landmark's DecisionSpace® software package for the construction of a three-dimensional stratigraphic framework for the Albian 18-22 HFS. The interpretations on the canyon-wall exposures provided the ability to create a 3D framework stratigraphic framework.

FACIES ASSOCIATIONS

There are 23 lithofacies assemblages that characterize depositional patterns across the carbonate ramp profile (Kerans et al., 1995). These facies can be further grouped into four facies tracts based on distinct sediment supply/water depth/energy regimes. The key facies tracts of the Devils River Formation include (1) the peritidal inner ramp, (2) the mud-dominated shallow-subtidal, (3) the high-energy shoal complex, and (4) the intrashelf basin (Kerans, 2002). The paleoecology of the rudist-bearing deposits has been of much interest on the Comanche Shelf, with studies looking at the Albian rudist reef communities across the Gulf of Mexico (Scott, 1990) and with focus on rudist buildups in the Devils River Formation (Scott and Kerans, 2004). Rudist distribution, type, and associated sediment bodies were integrated with a sequence stratigraphic framework by Kerans (2002) who demonstrated that strong facies partitioning exists between the highstand and transgressive systems tract of the last six Albian high-frequency sequences with respect to rudist assemblages and associated depositional facies.

The facies tracts of the Maverick ISB are dominated by high-energy shoal complexes and intrashelf basin facies in the simple upward-coarsening prograding lower shoreface-upper shoreface-foreshore depositional model. The Albian 19 deposits in the updip section of this study also contain well-developed mud-dominated shallow subtidal shelf environments. These three facies tracts and key lithofacies assemblages will be discussed in further detail below.

High-Energy Shoal Complex Facies Tract

Facies assemblages in this facies tract are dominated by caprinid-skeletal grainstones and rudstones that are indicative of wave agitation, mechanical breakdown of grains, and winnowing of mud, leaving a well-sorted skeletal sand facies. Sedimentary

structures include burrowing in lower sections, low-angle parallel current lamination, 5-10 cm thick planar-tabular crossbed sets, and in the upper portions of the facies assemblage, small-scale trough cross-stratification oriented at high-angle to the seaward dipping swash-laminated foreshore deposits. The sedimentary structures indicate shorelines that were either tide-dominated or wind-dominated. Variations were documented by Kerans et al. (1995) and Kerans (2002) between tidally dominated and wave-dominated facies successions for each of the high-frequency sequences. These high-energy ramp crest deposits grade laterally offshore into skeletal grain-dominated packstones, before transitioning into intrashelf basin facies. Three key lithofacies of the shoal complex facies tract are described below:

Caprinid-Peloidal-Skeletal-Grainstone (Fig. 6B): this facies consist of swash-laminated grainstone fabrics. The accretion stratified bedding dips seaward at 2-3° and the grains are well-sorted medium-grained size sand. The clast are primarily composed of peloids, foraminifera (miliolids), skeletal fragments (including caprinids, mollusks, and echinoderms), and rarer large (5-10cm) caprinid fragments. Peloids are well-rounded, and skeletal fragments are highly abraded with thin micritic rims. This facies passes downdip into trough cross-stratified peloid-skeletal grainstones (Kerans, 2002).

Caprinid-Rudstone (Fig. 6C): massive bedded with whole ~30cm caprinids and gravel-sized caprinid fragments. Matrix consist of coarse-sand to gravel-sized skeletal fragments that include rudist and mollusk. The coarse sand and skeletal fragments are well-rounded with micritc rims. Locally abundant peloids around large whole caprinids and filling the internal pallial canal. The original aragonite that composed the caprinid shells have been completely replaced by blocky calcite cements. This facies passes vertically into trough cross-stratified grainstones, and transitions downdip into crossbedded grain-dominated packstones (Kerans et al., 1995).

Peloidal-Skeletal Grain-dominated Packstone (Fig. 6D): the facies is composed fine- to medium-grained sand size peloids and skeletal clasts with tabular crossbed sets that are 5-10cm thick. There is an abundance of fine-grained sand sized, moderately rounded peloids and intraclasts. Skeletal clasts are predominantly rudist and mollusk fragments with well-developed micritic envelops. Moldic porosity is common and develops from late-stage fabric-selective dissolution of grains. This facies passes laterally into more distal heavily bioturbated peloid-skeletal mud-dominated packstones (Kerans et al., 1995).

Mud-dominated Shallow-Subtidal Facies Tract

The distinct facies within the mud-dominated shallow-subtidal shelf facies tract are massive condrodont-radiolitid mounds with geometries ranging from biostromal units that extend thousands feet to bioherms that range between 100-500 ft in diameter with well-developed flank beds (Kerans, 2002). The primary facies assemblages can be divided into bedded miliolid-gastropod grainstones to the mound/intramound facies. Downdip from the well-developed bioherms there is a distinct contrast and change in mound development. Mound facies assemblages on the Lower Pecos River are predominantly massive toucasid rudstones that form 2-4m biostroms. Three levels of mound development can be identified at Nine-Mile Bend (LP1) with primary mound builders of toucasid rudist. Occasionally, these mounds are capped by thin monopleurid rudstones and are surrounded by gastropod-miliolid packstones to toucasid skeletal packstones. The shallow subtidal facies tract in the outer ramp pass laterally into skeletal wackestones and mudstones in the intrashelf basin. The two key facies assemblages of the mud-dominated outer ramp deposits are discussed below:

Toucasid Rudstone: massive weathered toucasid rudstones that from biostromal 2-4m mounds and are predominantly composed of large 10-20cm toucasid rudist. These rudstones contain the largest observed toucasid rudist along the entire depositional profile of the Maverick ISB. The toucasid rudist are intact with dark brown thin wall structures. The matrix of this rudstone is a fine-grained mud-dominated fabric. This mounded facies assemblages is typically capped by bedded miliolid grainstones/packstones and passes downdip into a toucasid gastropod mud-dominated packstones (Kerans et al., 1995).

Toucasid Gastropod Packstone: thin to medium-bedded mud-dominated packstone to wackestone that is composed of toucasid rudist and high-spired gastropods. The matrix is fine-grained mud-dominated with an abundance of miliolid foraminifera. The toucasid rudist are a diagnostic fauna of the mud-dominated shallow subtidal facies tract. Toucasid rudist are typically 10 cm in diameter with thin dark brown peanut-shaped wall structures. The toucasid gastropod packstone can be surrounding larger toucasid rudstones and pass laterally downdip into skeletal wackestones of the intrashelf basin (Kerans et al., 1995).

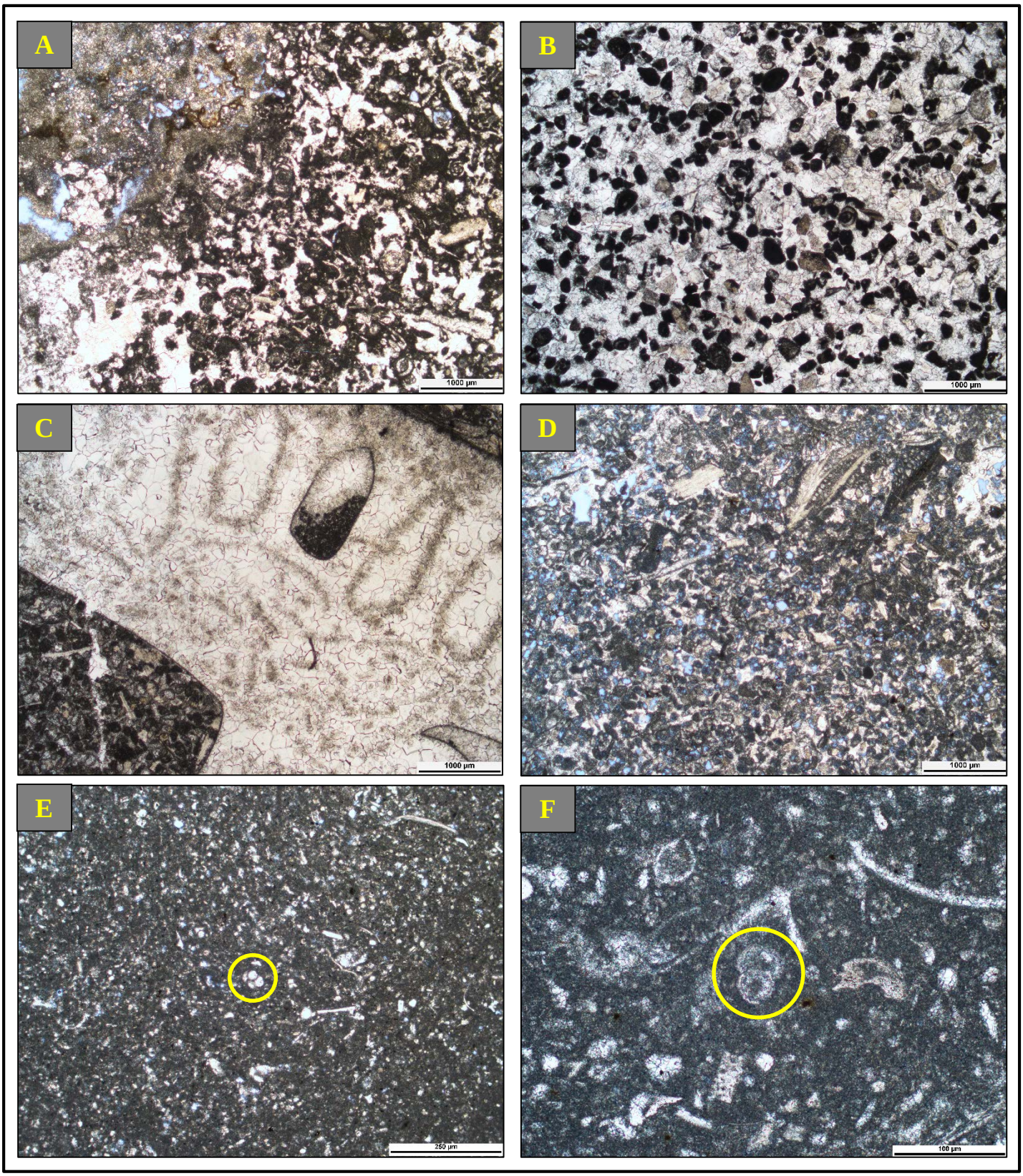

Figure 6: Representative photomicrographs of the key facies. Continued on next page.

Figure 6, cont. Representative photomicrographs of the high-energy shoal complex facies tract (A-D) and the intrashelf basin facies tract (E-F). Stratigraphic location of thin sections are shown on the stratigraphic column in Figure 7. A) Karst fabric with a miliolid-echinoid-peloid mud-dominated packstone. B) Peloid-skeletal-caprinid grainstone. C) Caprinid Rudstone with complete blocky calcite cement replacement of aragonite. Note the preservation and geopetal fill of the pallial canal of the caprinid. D) Peloid-skeletal grain-dominated packstone with moldic porosity generated by late-stage dissolution. E) Spiculitic-globigerinid mudstone, highlighted in yellow is a four chambered planktonic globigerina foraminifera. F) Foraminifera-skeletal wackestone with planktonic globigerinid foraminifera (yellow circle).

Intrashelf Basin Facies Tract

The accumulation of fine skeletal wackestones and planktonic foraminifera mudstones represent the dominant facies of the intrashelf basin facies tract. Higher energy facies of the intrashelf basin slope profile begin to condense around the Railroad Bridge where there is a lateral shift of facies to the recessive weathered, thin-bedded skeletal wackestones and globigerinid mudstones. At this transition, larger proportions of mud-dominated sediments containing planktonic foraminifera indicate that sediment accumulated in water depths of at least 30 m. Descriptions of the key lithofacies of the intrashelf basin facies tract are provided below:

Skeletal-foraminifera wackestone (Fig. 6F): nodular bedded tanish to white recessively weathered packages that are bedded at the scale of 10-30 cm. This facies contains an abundance of foraminifera and depending on location within the framework are dominated by planktonic or benthic foraminifera. There is also a major presence of thin-walled gryphaea mollusk fragments. This facies also contains minor fragments of echinoderms and gastropods. The skeletal-foraminifera wackestone transitions updip into either mud-dominated subtidal facies or higher energy shoal complexes. Downdip, this facies passes into globigerinid mudstones.

Spiculitic-globigerinid mudstone (Fig. 6E): nodular to slightly bioturbated bedding with an abundance of planktonic foraminifera (globigerinids), calcispheres, and sponge spicules. Bedding is 10-20 cm of darker grey to black recessively weathered packages. This facies transitions updip from skeletal wackestones and the presence of globigerinid foraminifera indicates sedimentation in deeper water, basin-center environments.

Vertical Facies Successions

Facies repetition is an import tool for accurate correlation and interpretation of sequence position in the subsurface (Kerans and Tinker, 1997). Cycle stacking patterns in

greenhouse settings are controlled by very low amplitude eustatic fluctuations. The result of this low amplitude changes in sea-level is cycle amalgamation, where the HFS-scale is the most resolvable cyclicity in the highstand systems tract (HST), and the cycle set scale is the highest resolvable during the transgressive systems tract (TST) (Kerans, 2002). A measured section from the Albian 21 HFS at LP4 (Fig. 1) displays ideal vertical facies succession within a wave-dominated foreshore-shoreface complex in the highstand systems tract (Fig. 7). The initial facies of the Albian 21 HFS is a massive burrowed peloidal skeletal grain-dominated packstone interpreted to have formed in lower-upper shoreface. This packstone transitions into a cross-stratified skeletal grain-dominated packstone that was deposited in the upper shoreface. The next facies is a caprinid rudstone with fragments of coarse rudist debris indicating a sedimentation style that is consistent and similar to a plunge-zone environment within the upper shoreface. The coarse rudist rudstone transitions into caprinid skeletal grainstones that displays upper shoreface trough cross-stratification. The final lithofacies assemblage is a peloid caprinid skeletal grainstone with seaward dipping accretionary stratification indicative of a foreshore complex. This ideal stacked section is capped by a brief period of exposure, with karst dissolution textures and dissolution pits, on the order of 10-30 cm, as supporting evidence.

The low-amplitude sea-level fluctuations have a major effect on cycle development and vertical stacking patterns in this ramp system. The low-angle dip of the depositional profile promotes the lateral breakout and shift of facies, rather than vertical trends (Kerans, 2007). This is a significant contrast to the well-defined stacking patterns observed in carbonate ramp systems that develop in transitional icehouse-greenhouse regimes, as shown by outcrop studies of the San Andres Formation in the Guadalupe Mountains by Kerans and Fitchen, (1995) along the Algerita Escarpment, New Mexico and Sonnenfeld and Cross, (1993) in Last Chance Canyon, New Mexico.

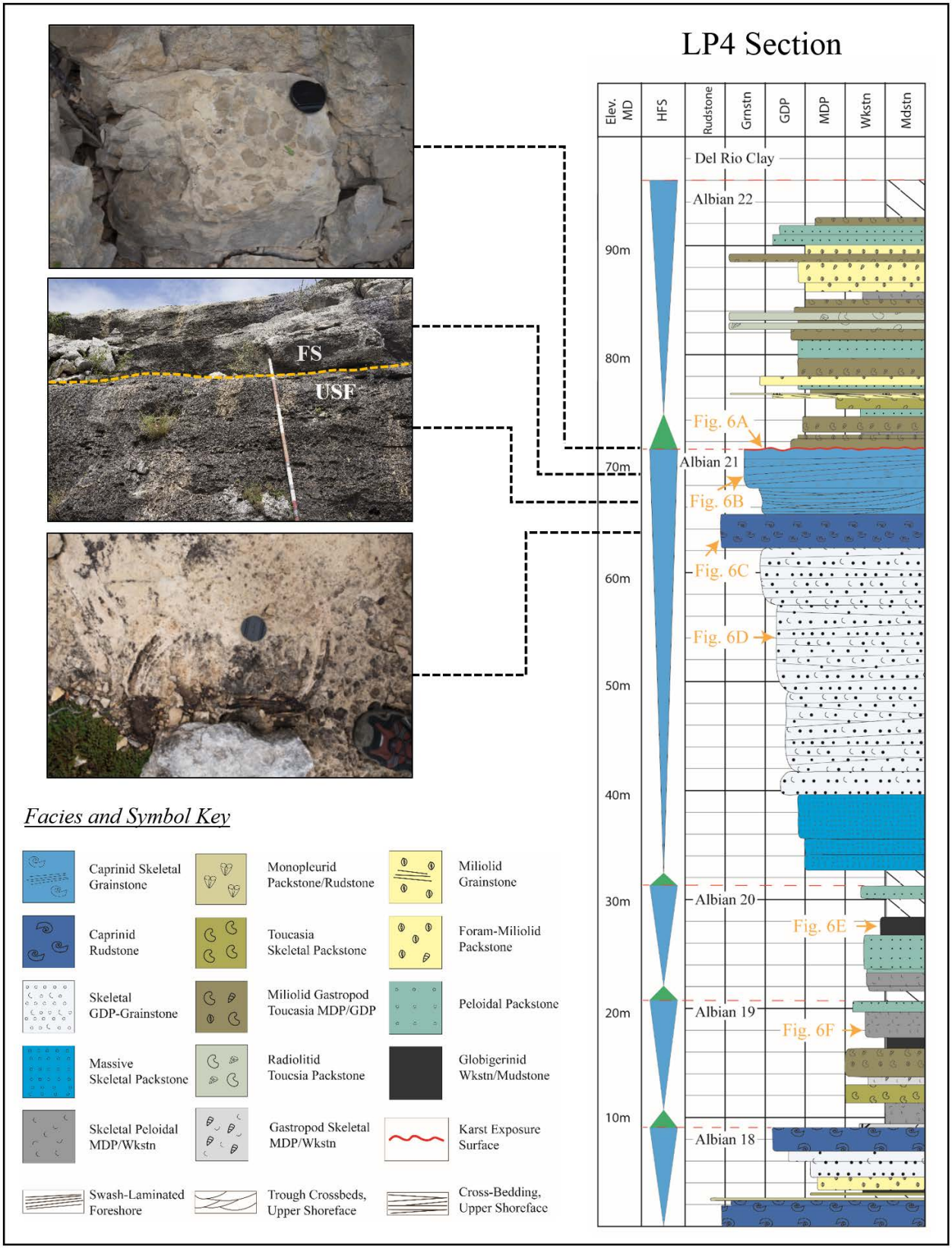

Figure 7: LP4 measured section. Continued on next page

Figure 7, cont. Measured LP4 Section demonstrating the condensed sections of the Albian 19 and 20 HFS and the ideal stacking patterns of a foreshore-shoreface complex that forms during the highstand systems tract of the Albian 21 HFS. Outcrop photos show transition from caprinid rudstone, upper shoreface trough cross-beds, laterally accreting swash laminated foreshore complex, and karst dissolution pit at the Albian 21 sequence boundary.

DEPOSITIONAL MODELS

The depositional history of the late Albian Maverick ISB has been described in systems tract-specific depositional models due to a high degree of facies partitioning that exist (Kerans et al., 1995). The depositional model for both the transgressive systems tract (TST) and highstand systems tract (HST) ramp systems can be subdivided into the inner, middle, ramp crest, and outer ramp environments (Burchette and Wright, 1992; Kerans and Fitchen, 1995) (Fig. 8). The TST depositional model consist of mud-dominated subtidal facies with well-developed (1-5 m thick) pancake-shaped radiolitid-chondrodont buildups. In this study, the buildups are biostromes that are dominated by toucasia rudstones that develop in outer shelf environments, and are observed at Nine Mile Bend (LP1) and Deadman's Canyon (LP2) (Fig. 8b). A contrast in the depositional styles for the HST model is based on observations at the ramp crest for each high-frequency sequence. Deposits along the northern margin of the Maverick ISB can be described as either wave-dominated or tide-dominated shoreline environments (Fig. 8a). Through detailed lateral facies mapping Kerans (2007), showed that the grainstones of the Albian 19 HFS form as part of a lagoon-inlet-barrier complex. The evidence for this is observed at Painted Canyon (Fig. 1) where paleocurrent data indicates a bimodal north-south (basinward) exchange of flow and a lower set of sigmoids that have depositional dips that build to the west, perpendicular to the ISB (Kerans, 2007). In this investigation on the lower Pecos River, the ramp crest of the Albian 21 HFS is interpreted as a wave-dominated shoreline with well-developed laterally accreting foreshore and shoreface grainstones.

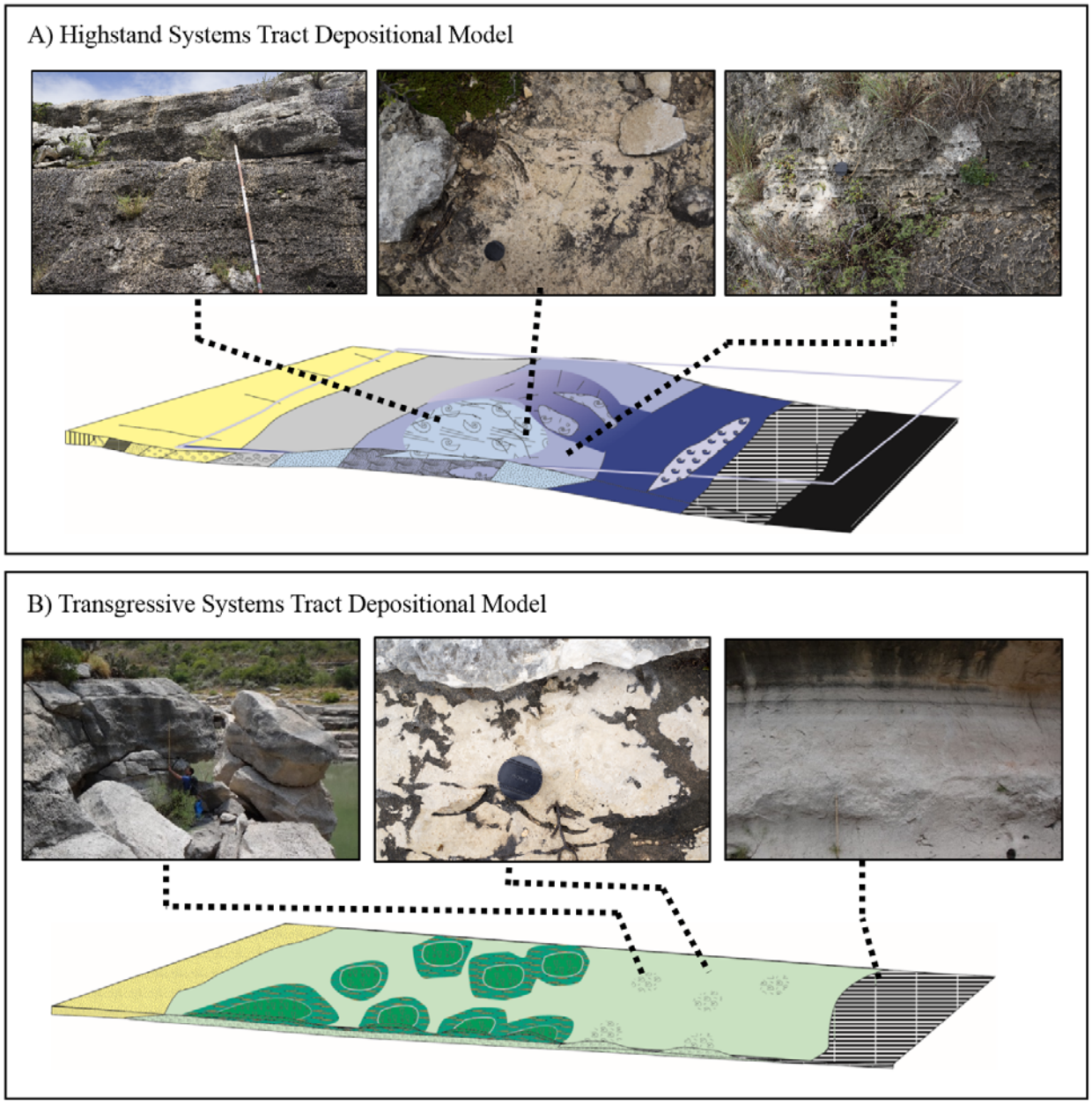

Figure 8: Depositional models for the Late Albian Maverick ISB. Continued on next page

Figure 8, cont. Generalized depositional model for the Late Albian high-frequency sequences. A) Highstand systems tract model highlighting both the wave-dominated foreshore-shoreface model and the tide-dominated tidal inlet model. B) Transgressive systems tract model showing the outer ramp toucasid biostromes that pass downdip into skeletal wackestones. Outcrop photos are provided for key elements of the generalized depostional models. Modified after Kerans, (2002).

STRATAL GEOMETRIES AND FACIES PATTERNS

Using data from the five measured sections LP1-LP5 (Fig. 1) and the digital outcrop model, 3D surfaces were interpreted for the lower Pecos River Canyon (Fig. 9). HFS surface boundaries were tied to the LP1-LP5 sections and previous sections of Kerans et al (1995) and Kerans (2002). Integration of facies data from the measured sections to dip-angles from the 3D modeled surfaces allowed refinement of a 2D dip-oriented cross-section showing precise lateral facies transitions relative to the sequence stratigraphic framework (Fig. 10). The interpretation and distribution of facies within the sequence stratigraphic framework will be discussed for this study in terms of an updip section from Nine-mile Bend to Deadmans Canyon, a transitional section around the railroad bridge, and the intrashelf basin section at the Highway 90 Bridge (Fig. 1).

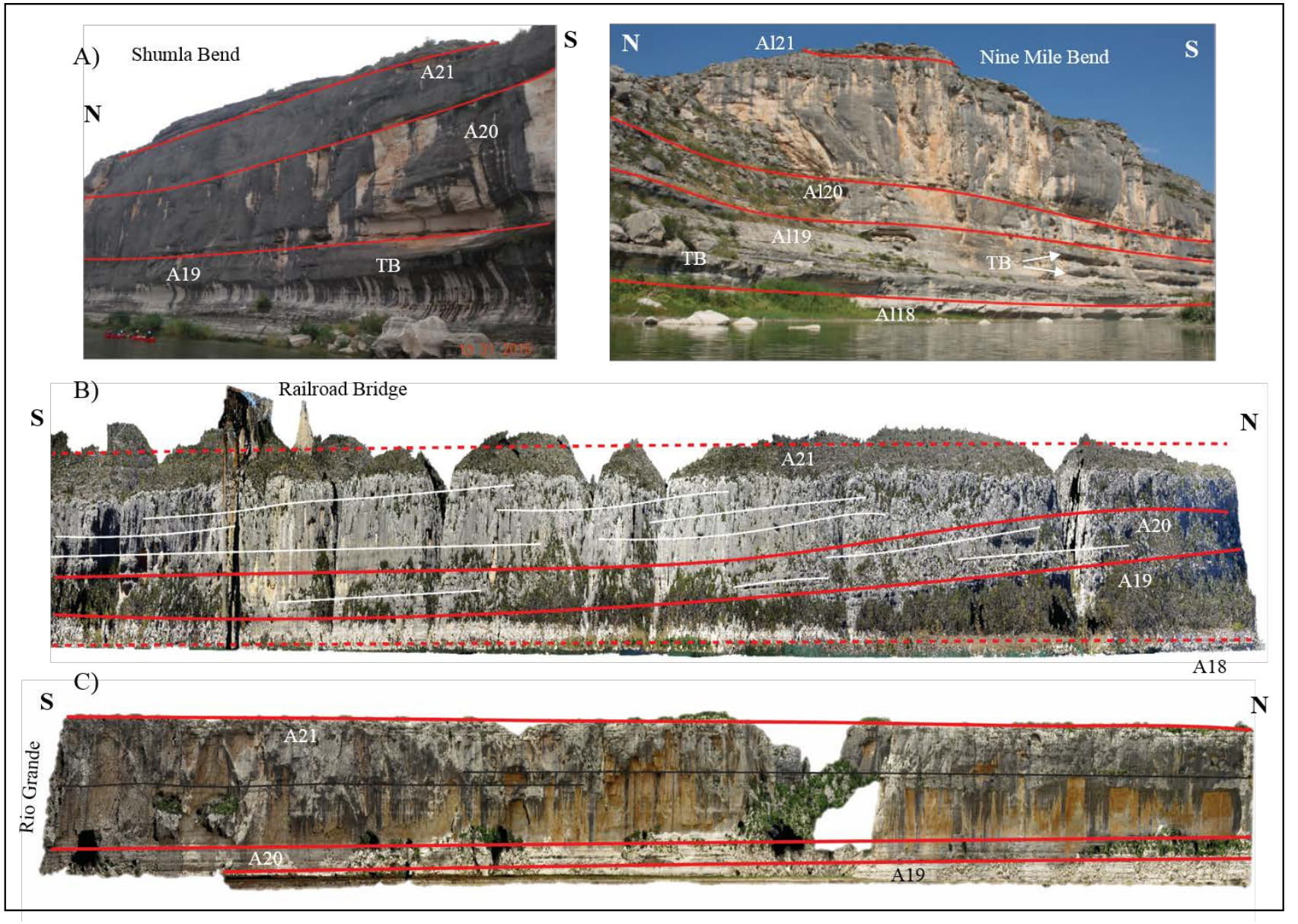

Figure 9: Interpretation of the Albian 18-21 HFS boundaries. Continued on next page.

Figure 9, cont. Interpretation of the Albian HFS from photos and the digital outcrop model. A) Shumla Bend – Nine Mile Bend, highlighting the initial development of the Albian 21 HFS. Note the multiple levels of toucasid biostromes (TB) in the Albian 19 HFS. B) 10x exaggerated panel from the digital outcrop model (DOM). Showing the downlap of the Albian 19 and 20 HFS, dip-angles are on the order of 0.3°. C) 2x vertically exaggerated panel from the DOM demonstrated the condensed intrashelf basin facies of the Albian 19 and 20 HFS and the large prograding grainstone of the Albian 21 HFS.

Updip Section (Nine Mile Bend-Deadmans Canyon)

The Nine-Mile Bend section, which represents the most updip section of this study, it is a total of 110m thick, and covers the Albian 18-22 sequences. It contains the thickest section (53m) of the Albian 19 and 20 HFS observed on the lower Pecos River. The most striking component of the updip section is the development of a major peloidal skeletal grainstone that expands within a short distance along dip (200m) and can be traced from an approximately 10m thick section at Shumla Bend to a 25m thick section at the Nine-Mile Bend section (LP1) (Fig. 9A) before expanding to 35m at the LP2 section. The facies assemblages observed in the updip section contain an initial skeletal-peloidal packstone that deepens into multiple packages of biostromal toucasid mounds. There are three well-developed outcrop levels of the toucasid rudstone facies with a thickness of 2-3m that are capped by bedded gastropod miliolid packstones at the LP1 section. The initial skeletal packstone is interpreted to be a shallow water facies that marks the top of the Albian 18 HFS, and the deepening into toucasid rudstone (mud-dominated shallow subtidal) facies represent the transgressive systems tract of the Albian 19 HFS. The toucasid mounds shallow into caprinid-skeletal packstones that are prograding over the lower energy buildups. This shallowing event and shift to higher energy is interpreted to be the highstand portion of the Albian 19 HFS. The HST portion of the Albian 19 significantly thins (12m) over a 1km in dip-distance from Painted Canyon (Fig. 1; Kerans et al, 1995). At Deadmans Canyon (LP2) there is a sharp contact with a 1m caprotinid mud-dominated packstone/rudstone that has evidence of local microkarst development along the same contact updip (Kerans, 2007). The caprotinid rudstone is then followed by an 18m thick cross-bedded peloid skeletal grainstone that is capped by a 3m thick caprinid rudstone. Above this contact there is a deepening back into a 1m caprotinid rudstone that is followed by a 35m thick cross-bedded peloid skeletal grainstone with the upper 5m consisting of

caprinid rudstones and swash-laminated caprinid skeletal grainstones. The development of the local microkarst below the first caprotinid rudstone is interpreted as a period of brief exposure and the top of the Albian 19 HFS. The Albian 20 HFS is missing a significant TST-dominated facies assemblages and the initial floodback is marked by a subtidal caprotinid rudstone and thin skeletal wackestone. The 18m peloid skeletal grainstone that shallows and progrades over the caprotinid rudstone is interpreted as the HST of the Albian 20 HFS. The major cliff former of the 35 m peloid skeletal packstone with caprinid rudstones is interpreted as the forced regressive HST of the Albian 21 HFS. The Nine-Mile Bend section is the first portion of the river where the Albian 21 HFS becomes the primary contributor to sediment proportions. Overall, the sedimentation patterns observed in the updip section at Nine-Mile Bend and Deadmans Canyon is a higher energy grain-dominated system.

Transitional Section (Railroad Bridge)

The areas around the Pecos River Railroad Bridge (LP3-LP4) represents the transitional section, where the grain-dominated sediment observed in the updip section begin to laterally shift into skeletal wackestones/mudstones of the intrashelf basin. The transitional section is a total of 96m thick and covers the Albian 18-22 high-frequency sequences. The key observation in this part of the slope profile is the 18m thin-bedded package of intrashelf basin facies that has condensed from over 50m thick rudist-dominated assemblages 7.5 km updip at Painted Canyon (Kerans et al., 1995). The downlap and condensing of the Albian 19 and 20 HFS sections can be traced along dip from Deadmans Canyon past the Railroad Bridge (Fig. 9B). The facies assemblages documented in the transitional section at LP4 consist of an 8m thick package with two levels of caprinid rudist buildups on the scale of 3 meters. The lower buildup of caprinid rudstones is capped by 20

cm monopleurid rudstone. These caprinid rudstone buildups are directly overlain by an 18m thick unit of recessively weathered, slope-forming beds that contain facies dominated by peloidal toucasid mud-dominated packstones/wackestones, skeletal-foraminifera wackestones, and spiculitic-globigerinid mudstones. The shallow-water high-energy caprinid rudist are interpreted to represent the highstand systems tract of the Albian 18 HFS. The condensed section of 18m thick intrashelf basin facies represents the entire deposition of the Albian 19 and 20 high-frequency sequences. The condensed section shallows into a 42 m thick ideal vertical succession that consists of burrowed massive peloid grain-dominated packstones to cross-stratified peloid skeletal packstone/grainstones. The cross-stratified grain-dominated packstones pass into caprinid rudstones that are capped by a 3 m thick peloid skeletal grainstone with trough crossbeds. The entire upper 2 m of this interval is a swash-laminated caprinid-peloid-skeletal grainstone that is capped by a well-developed karst exposure surface that contains 10-30 cm dissolution pits. The 42 m thick ideal vertical succession is interpreted to represent high-energy ramp crest facies that were deposited in a wave-dominated foreshore-shoreface environment. This forced regressive interval represent the highstand of the Albain 21 HFS and downlaps over the condensed sections of the Albian 19 and 20 HFS. The karst exposure surface at the top of this interval is the Albian 21 sequence boundary, which separates the prograding Albian 21 HFS from the backstepping toucasid-miliolid packstone dominated facies of Albian 22 HFS.

Intrashelf Basin Section (Hwy. 90 Bridge)

In the most distal section of this study, at the confluence of the Lower Pecos River and the Rio Grande, the Highway 90 section is a total of 80 m thick and covers the Albian 18-22 high-frequency sequences. The most impressive observation along the growing

proportion of intrashelf basin facies and the major cliff former that consist of a 42 m thick unit of skeletal peloid packstone/grainstones. At section LP5, there is a small exposure of caprinid rudstone at the base of the Highway 90 Bridge. This caprinid facies assemblage is directly overlain by 10 m of intrashelf basin deposits. These deposits are comprised of peloid mud-dominated packstones, skeletal wackestones, and globigerinid mudstones that are indicative of deposition in deeper water conditions. The small exposure of caprinid rudstone is interpret to represent the top of the Albian 18 HFS. The deposition of the Albian 19 and 20 HFS are contained within the condensed 10 m of skeletal wackestones and globigerinid mudstones. This 10 m condensed section is overlain by a 20 m package of massive peloid skeletal wackestones and packstones that transition into cross-stratified skeletal grain-dominated packstones. Near the top of this 42 m sequence there is a 2 m reworked caprinid fragment rudstone. This sequence is interpreted to represent shallow-water foreshore-shoreface environments of the forced regressive Albian 21 HFS. At the sequence boundary of Albian 21 HFS there is evidence of exposure and heavily micritized grains that are similar to the foreshore complex documented updip at the LP4 section. The 42 m thick package of skeletal packstones/grainstones is overlain by a 24 m mixed succession of caprotinid/caprinid rudstones, miliolid gastropod packstones, gastropod toucasid packstone/rudstone, peloid skeletal packstone/wackestones. This retrogradational interval is interpreted to represent the backstepping Albian 22 high-frequency sequence. The sequence boundary of the Albian 22 HFS is a bored firmground that is most likely marine in origin (Kerans et al., 1995). The Devils River Formation at the Highway 90 Bridge is unconformably overlain by the Cenomanian Del Rio Clay and Buda Limestone.

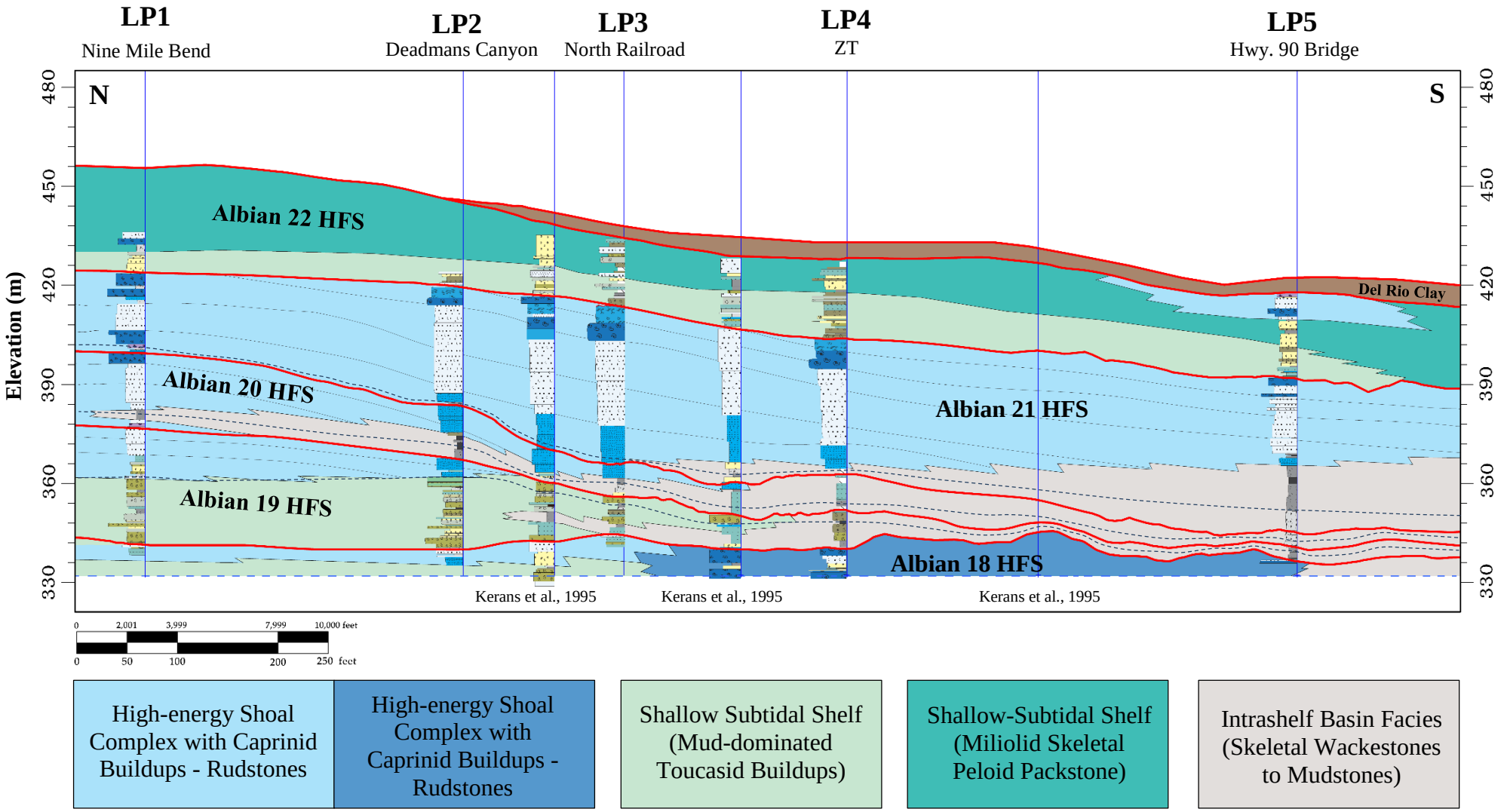

Figure 10: High-resolution sequence stratigraphic framework for the Lower Pecos River. Sequence boundaries (in red) were mapped from the digital outcrop model and facies tract distributions were correlated within the DOM interpreted HFS framework using the stratigraphic measured sections. Note the visual change in the stratal geometries also marks the transition from outer ramp facies into intrashelf basin skeletal wackestones and globigerina mudstones.

STRATIGRAPHIC ARCHITECTURE

The stratigraphic model focused on characterizing the stratal geometries of the Albian 18-21 high-frequency sequences. Construction of the 3D stratigraphic model integrates data interpreted from the digital outcrop model and the five sections that were measured along the lower Pecos River. The study also mapped the top of the Albian 22 HFS from NAIP 2ft aerial imagery and extracted elevation values from the USGS 10m National Elevation Dataset. The Albian 22 HFS was then gridded over a 40 sq. km area of the Lower Pecos River, and corrections were applied using differentially corrected GNSS field-collected control points. The Albian 22 HFS surface was used to guide the gridding of the surfaces using top-down conformance relationships for the Albian 18-21 HFS away from interpretations traced along the canyon. The dip angles of the ramp profile were then extracted from structure contour maps created for each of the HFS, using similar surface attribute extraction methods used in subsurface datasets. The Albian 18 HFS is a very flat surface with dips averaging 0.08 degrees with locally higher dips in areas with a higher concentration of rudist mounds. The primary goal of this study was to capture a change in stratal geometry at the shelf-to-basin transition and lateral shift of facies from grain-dominated facies on the ramp into mud-dominated ISB deposits for the Albian 19 and 20 HFS (Fig. 11). The Albian 19 HFS has an average dip angle of 0.2 degrees with a bimodal distribution of dip angles that indicates the shelf-to-basin transition. The dip angles over this transition decrease from 0.4° to dip angles of 0.15°. The Albian 20 HFS depositional profile is at a higher angle than the Albian 19 HFS and has average dips of 0.3 degrees. A bimodal distribution of dip angles is also observed in the Albian 20 HFS with ramp dip angles at 0.6° and an intrashelf basin profile of 0.2°. The dip-angle histogram for the Albian 21 HFS ramp morphology shows a unimodal distribution of angles that average 0.33

degrees. The unimodal distribution of dips within the Albian 21 HFS results because the shelf-to-basin transition occurs approximately 15-30 km basinward of this investigation. The interpretation of the shelf-to-basin transition can be shown on the modeled structure contour maps along with a comparison of dip angle, dip width, and P/A ratios (Fig. 12).

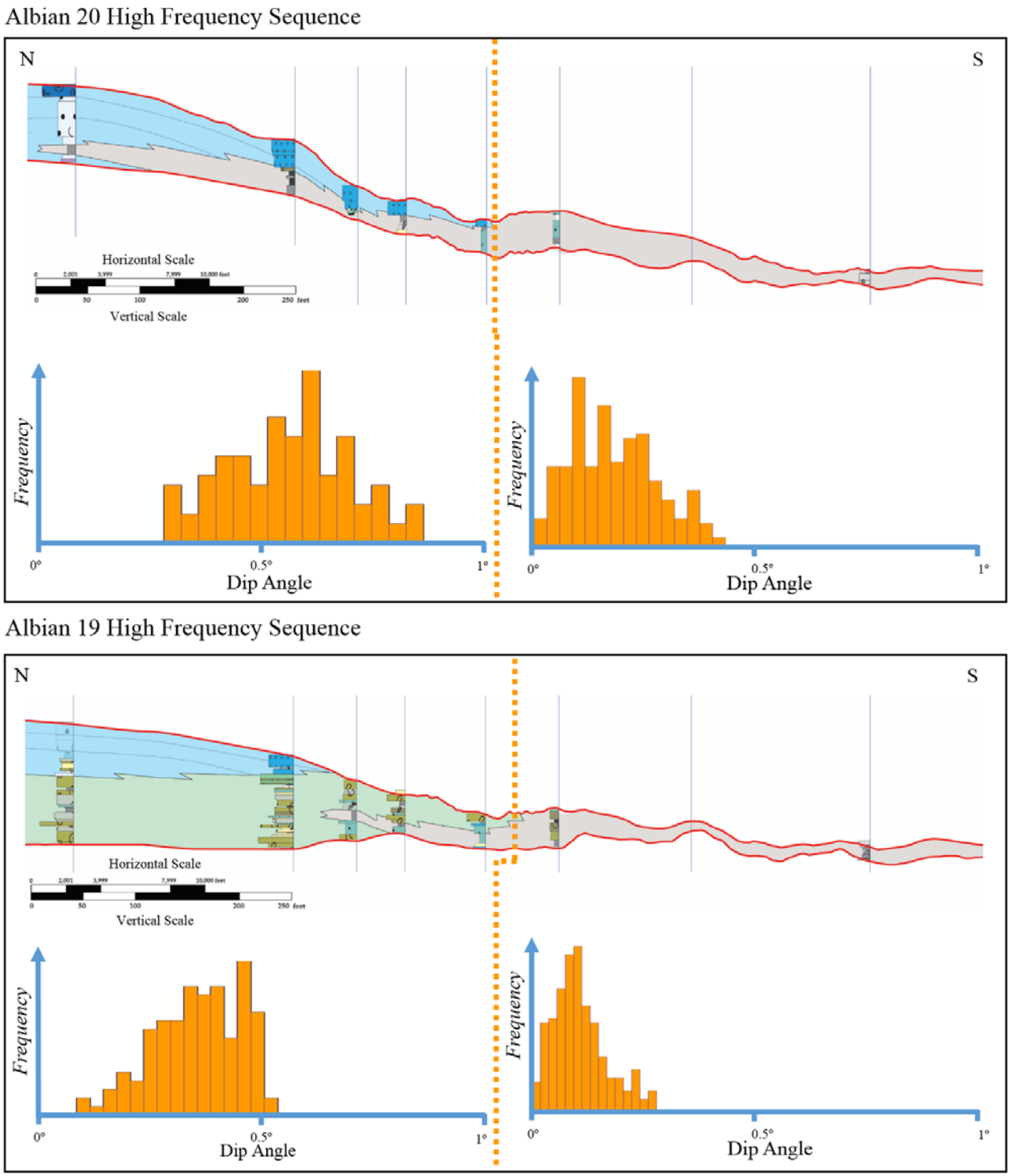

Figure 11: Relationship of the lateral facies transition to changes in dip angle of the depositional profile for the Albian 19 and 20 high-frequency sequences. As there is an increase in dip of the depositional profile sedimentation shifts from mud-dominated intrashelf basin facies into higher energy grain-dominated assemblages.

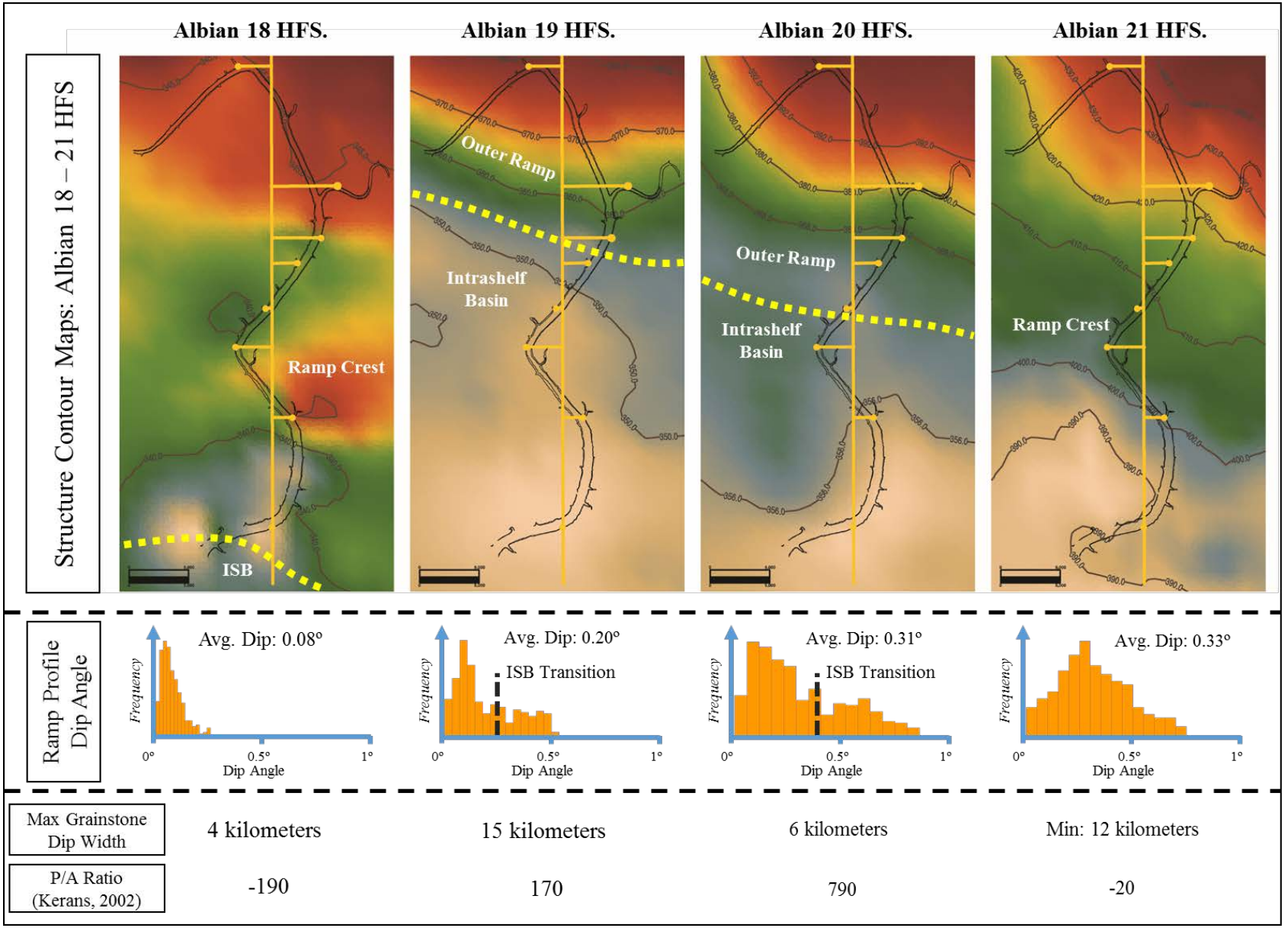

Figure 12: Structure contour maps with interpreted shelf-to-basin transitions. Continued on next page.

Figure 12, cont. Structure contour maps with interpreted shelf-to-basin transitions. Comparisons of dip angle, dip width, and P/A ratios are made for each of the high-frequency sequences. Note that the Albian 21 HFS ramp crest is situated over the condensed transition of the Albian 19 and 20 HFS. The Albian 21 HFS shelf-to-basin transition is approximately 20 km basinward of this study area.

DISSCUSSION

This study suggest that the origin of the Late Albian Maverick Intrashelf Basin resulted from subtle topographic expression (1-3 m) that lead to the divergence of sediment accumulation rates within the carbonate factory. This model of ISB evolution is similar to that proposed for the Bab Intrashelf Basin and the ISB development with the Savark-Natih Formations (Droste, 2010; Razin et al., 2010; Van Buchem et al., 2002a). Through detailed sequence stratigraphic analysis it can be demonstrated that eustatic fluctuations and accommodation are the most important factors that control the depositional profile of ISB ramp systems. While the drivers and dynamics for the evolution of intrashelf basins is well-documented, there is still a lack of understanding behind the primary controls on the origin and location of intrashelf basin systems.

Evolution of the Late Albian Maverick ISB

The dynamics of the Late Albian Maverick ISB evolution can be characterized in four main stages as demonstrated in Figure 13. The first stage of evolution is represented by the Albian 18 TST, where the rate of sediment accumulation is equal across the platform top. In the HST stage of the Albian 18 HFS the initial development of caprinid rudist buildups provides the earliest evidence of topographic expression for the Maverick ISBs. The second stage, is the deposition of the Albian 19 and 20 HFS that are characterized by rapid aggregation of the ramp margins, and demonstrate the first major differentiation between the margin and ISB. The deposits across the ramp margin consist of facies assemblages that are dominated by radiolitid-condrodont-toucasid rudist buildup in the transgressive system tracts and caprinid grainstone-rudstones in the highstand system tracts.

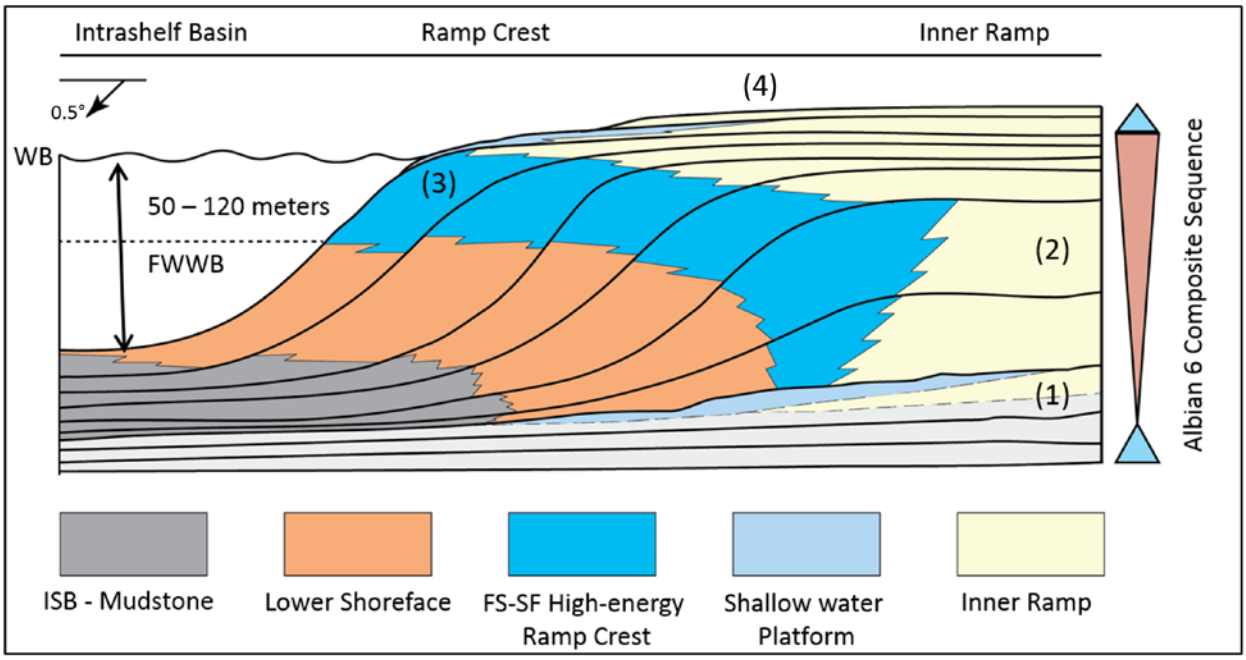

Figure 13: Idealized sequence stratigraphic evolution for the Maverick Intrashelf Basin. This idealized model highlights the key stages of ISB development. 1) Uniform aggradation of the platform top and development of initial topographic expression 2) aggradation and formation of the ISB shelf-margin (3) progradation and infill into the basin 4) final backstep onto the ISB margin (Kerans, 2002; Razin, 2010)

The third stage, is highlighted by the Albian 21 HFS that consist of a major progradational wedge that downlaps and infills over the Albian 19 and 20 HFS. The final stage of Maverick ISB deposition is characterized by the backstepping deposits of the Albian 22 and 23 HFS.

Controls on Origin and Evolution of ISBs

The origin of intrashelf basins is thought to result from small differences in topography that results in the development of differential rates of sedimentation. The creation of minor topographic expression is enough to trigger the formation of intrashelf basin deposits during periods of relative sea-level rise (Razin et al., 2010). The differential topography can result from antecedent topography, differential subsidence, tectonic influence, or the construction of subtle mound geometries. In the case of the Maverick ISB, the likely driver behind the initial positive topographic expressions is the development of caprinid rudist mounds that develop after the major maximum flooding event of the Albian 6 CS (Albian 18 MFS - Dr. Burts Bed; see Rose, 1972) and within the HST of the Albian 18 HFS. The rudist complex in the Albian 18 HFS spans 4 km in dip width and bedding is characterized by large-scale hummocks that develop on the order of 1-3 m.

Another possible explanation for the origin of intrashelf basin systems could be ecoeustatic drivers that cause the carbonate factory to shutdown, leading to broad areas of subdued sedimentation rates. During the Cretaceous, there was a tendency for ocean circulation to become stagnant and result in the stratification of temperature, salinity and oxygenation of the water column (Meyer and Kump, 2008). Several Ocean Anoxic Events are recognized across the Comanche Platform, with well-constrained and documented evidence for the major Aptian OAE1b and Cenomanian-Turonian OAE2 events (Phelps et al., 2014). The exact location of the OAE 1d event on the Comanche shelf is not well-

confined, but recent studies have placed the event in the late Albian, around the same time that the Maverick ISB was developing (Phelps et al., 2015).

The primary driver of intrashelf basin evolution is accommodation through its control on the morphology of the ramp profile (Razin et al., 2010). The dip angle of the depositional profile influences sedimentation by controlling the energy of the system. Lower angle profiles result in lower energy regimes and sedimentation results in mud-dominated facies assemblages typical of intrashelf basin deposits, whereas higher angle profiles promote higher energy systems that result in grain-dominated facies assemblages (Droste and Van Steenwinkel, 2004; Razin et al., 2010). There is also a connection between carbonate sediment type and the ramp angle, increasing the dip-angles results in a shift from foraminifera skeletal wackestones and globigerinid mudstones into rudist-bearing, bioclastic grain-dominated assemblages. Finally, on a large-scale the volume of carbonate sediment production is much greater in higher angle depositional profiles, but the volume/distribution of sediments between different HFS is controlled by the evolution of the ISBs. This is demonstrate by the Albian 20 HFS having a greater average dip angles than the Albian 19 HFS, but the grainstone dip-width of the Albian 20 HFS is nearly 9 km less than the Albian 19 HFS.

Dip Angle of the Depositional Profile and Facies Variability

Accommodation is the major control on the dip angle of the depositional profile and is the key influence on depositional patterns observed on carbonate ramp systems transitioning into intrashelf basin deposits. Increase in depositional dip angles promotes an increase in energy and causes the transition of sedimentation from a low-energy mud-dominated system into a grain-dominated system (Droste and Van Steenwinkel, 2004; Razin et al., 2010). This increase in energy leads to higher sedimentation rates and builds

the ramp margin of ISB systems through aggradation. The increase in energy that results from an increase in water depth of the basin system, combined with an appropriate ramp morphology promotes the exchange of tidal currents which leads to deposition of facies in a lagoon-inlet-barrier complex as documented in the lower angle (0.2°) HST of the Albian 19 HFS. In similar HST settings of the Albian 20 and 21 HFS greater dip angles (0.3°) promote an even higher-energy wave-dominated environment that leads to the deposition of deposits within a foreshore-shoreface complex.

Similar relationships between stratal geometries and facies have been documented in the Natih-E formation (Droste, 2010; Droste and Van Steenwinkel, 2004) and the Shuaiba Formation (Van Buchem et al., 2002a). Dip-angles across the margin of intrashelf basins can range from less than 0.5° and up to 35°. The deposition of steeper angle clinoforms along the ISB margin have been attributed to a contrast between highstand versus lowstand development (Droste and Van Steenwinkel, 2004). However, this relationship of subtle angles in depositional profile developing as a lowstand wedge is not observed in the Maverick ISB. Instead, the depositional profile of the Maverick ISB is less than 1 degree throughout the entire evolution of the system. These relationship observed between changes in dip angles and facies distributions are directly analogous to the Bab Intrashelf Basin of the Shuaiba Formation where dips range from lower energy deposits with 0.1° to higher-energy deposits with 5° dip angles (Droste, 2010; van Buchem et al., 1996). It is also important to note that while the morphology of the ramp profile along the northern margin of the Maverick ISB never exceeds 1°, there is variability that occurs along the margin. There have been documented dip angles that reach 20° on the western margin of the Maverick ISB in Mexico (Osleger et al., 2004). This increase in dip angle of the depositional profile occur as a function of greater accommodation and much higher energy regimes along that portion of the ramp margin.

CONCLUSION

Documenting the shelf-to-basin transition of the Late Albian Maverick Intrashelf Basin provides an analog for unraveling the stratigraphic complexity at a higher-resolution than any subsurface dataset. Understanding the shelf-to-basin transition of intrashelf basin systems has important implications at the reservoir scale. Knowing the distribution/variability between highstand grainstone facies to intrashelf basin deposits and the relationship to the geomorphic expression at the shelf-to-ISB transition will help improved reservoir understanding of ISB petroleum systems.

Interpretation of a high-resolution digital outcrop model and vertical measured sections show that lateral facies transitions of grain-dominated facies into skeletal wackestones/glogbigerinid mudstones occur across a decrease in the depositional slope angle by at least 25 percent for the Albian 19 and 20 high-frequency sequences. The condensed section that represents the transition into intrashelf basin facies of the Albian 19 and 20 HFS occurs 7.5-8 km downdip from the ramp crest. Documentation of Albian 19 and 20 HFS along the Lower Pecos River confirms the relationship between the dip angle of the ISB slope and lateral transition of facies across the depositional profile. Higher-angle dips of the slope profile promotes sedimentation of grain-dominated facies assemblages found along the ISB margins and the decrease in slope angle marks the transition to mud-dominated ISB facies with lower-angle dip profiles. The forced regressive Albian 21 HFS that represents the infills stage of ISB evolution fills the available accommodation space created by aggradation of the ISB margins, and with a slope profile of 0.33° has the greatest depositional dips documented along the Maverick ISB.

The depositional models developed for the highstand and transgressive systems tract for the Maverick ISB ramp system by Kerans (2002) accurately characterizes lateral

facies changes observed on the lower Pecos River. The highstand wave-dominated foreshore-shoreface model is represented in an ideal facies succession at the ramp crest of Albian 21 HFS. The highstand of the Albian 18 HFS demonstrates the first evidence of positive topographic expression that helps drive the separation of sedimentation rates that leads to the development of an intrashelf basin system. The Albian 19 HFS grainstones have a dip width of 15 km with average depositional profile of 0.2° and aggradationally stack to form the ramp margin of the Maverick ISB. The Albian 20 HFS have a greater averages depositional dip of 0.3° with shorter, 6 km dip-widths of HST grainstones. The Albian 21 is a forced regressive progragrading wedge that steps basinward nearly 30 km. The minimum dip width of the Albian 21 is 12 km with a depositional profile that averages 0.33°.

A key observation of this study is the comparison between similar constructional differential-accumulation driven intrashelf basins. The Maverick Intrashelf Basin has an origin and evolution that is comparable to documented intrashelf basins in the Middle East. The observations of the Maverick ISB supports the constructional differential-accumulation model. This is important because it highlights the ability of the carbonate factory to develop a topographic response to eustatic fluctuations and the control that accommodation exhibits on the evolution of these systems through subtle changes in depositional slope angles. The constructional development of the Maverick Intrashelf Basin also provides insight to the processes that formed the Fort Stockton and East Texas Intrashelf Basin systems.

APPENDIX

The purpose of this appendix is to provide additional figures to include supplementary information on the documentation of the Shelf-to-ISB transition of the Late Albian Maverick Intrashelf Basin presented in Chapter 1. Additional material will include all measured sections, additional field photographs, interpretation from the DOM, stratigraphic architecture, and several cross-sections from the Middle East and the Comanche Platform.

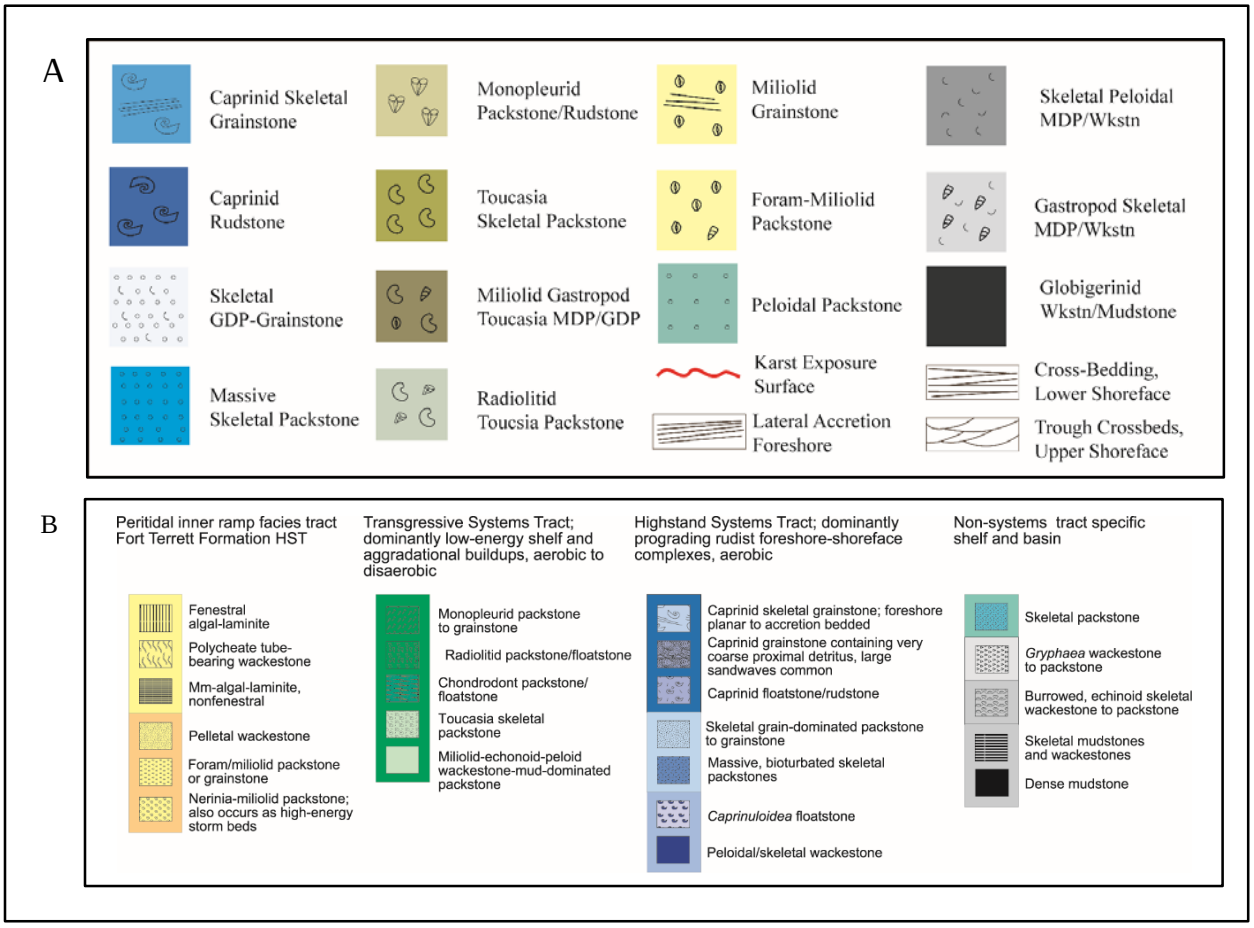

Figure 14: Facies key for the Pecos River. A) This study B) Kerans, (2002).

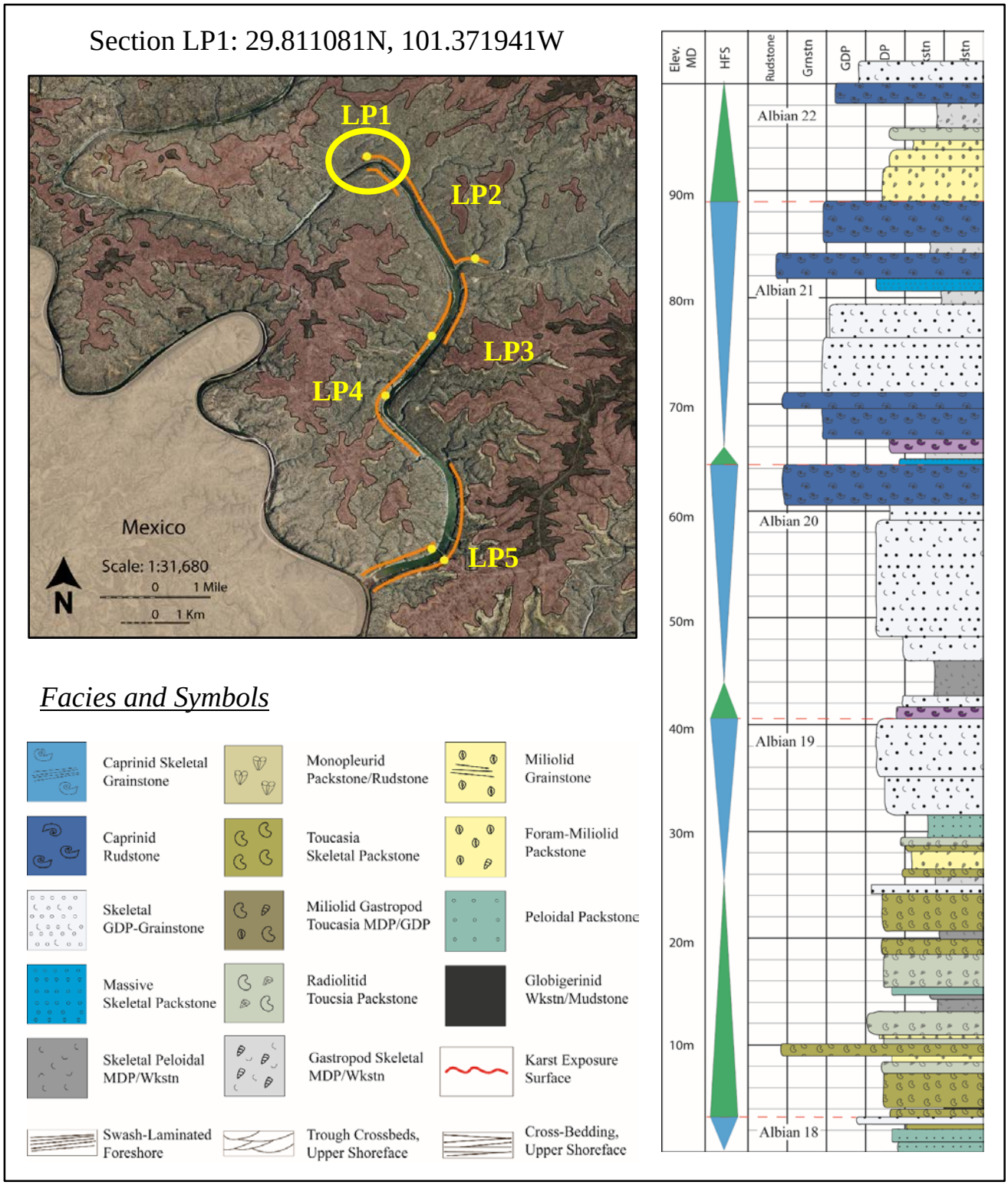

Figure 15: Measured section LP1, Nine Mile Bend.

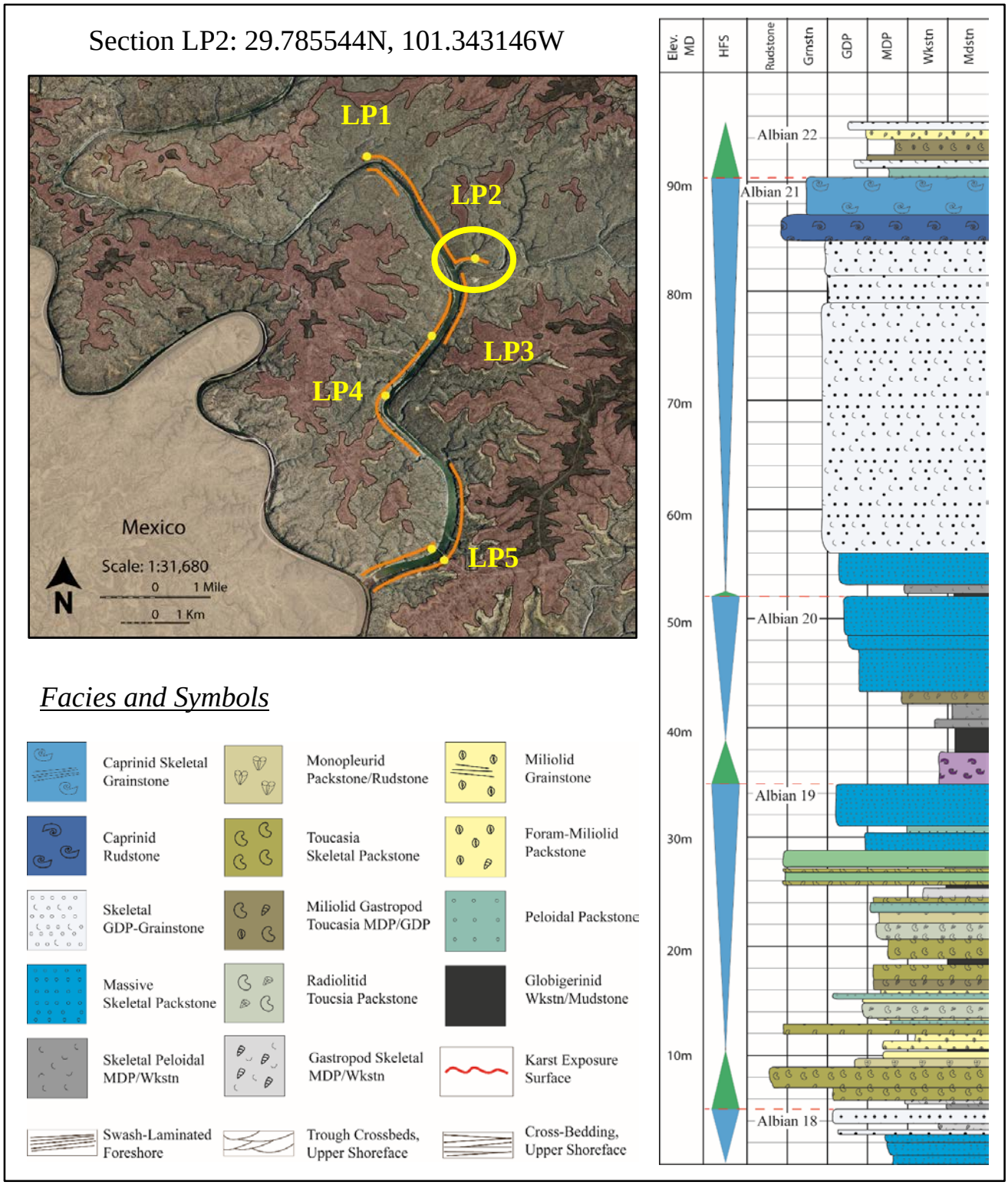

Figure 16: Measured section LP2, Deadmans Canyon.

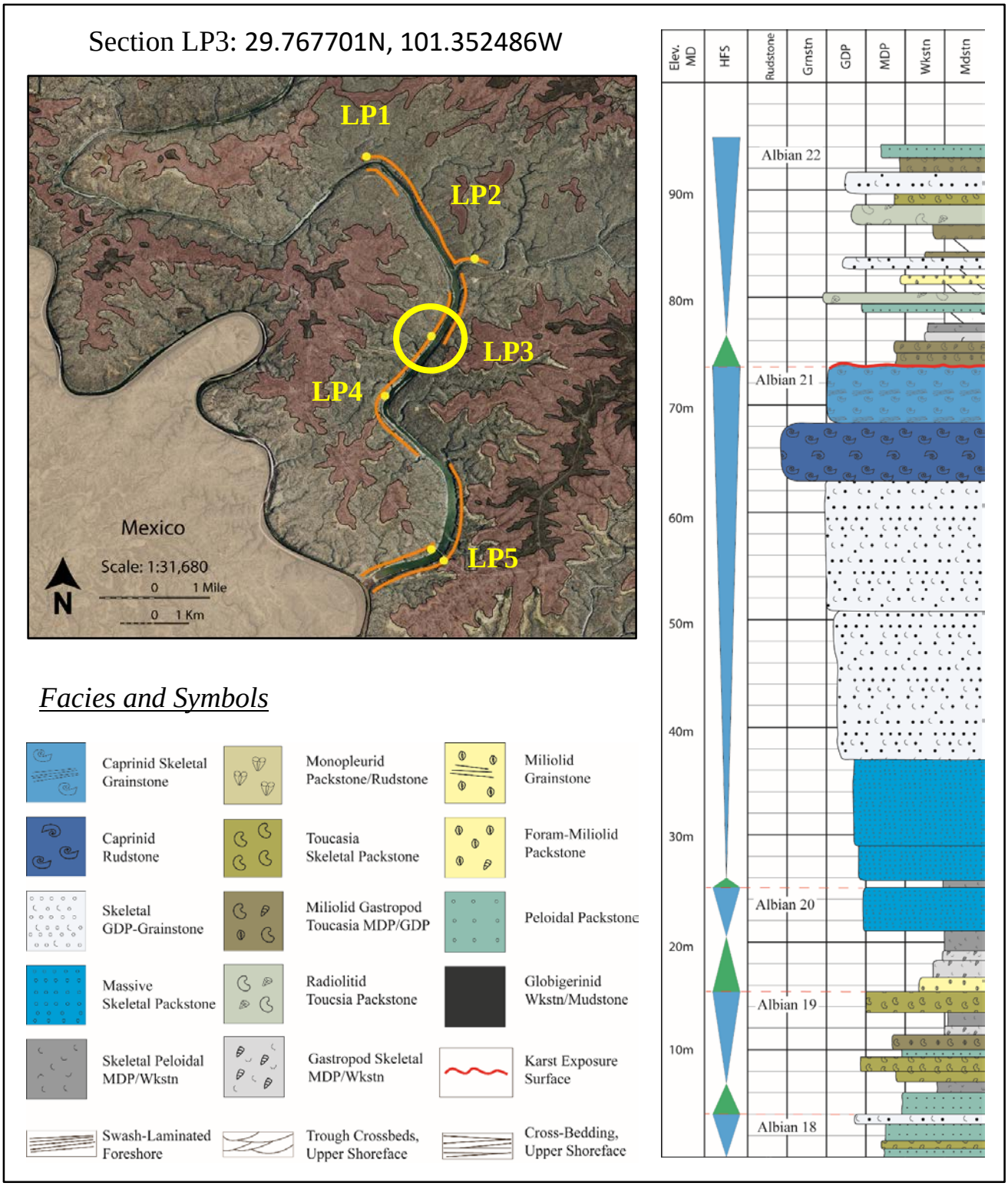

Figure 17: Measured section LP3, North of Railroad Bridge.

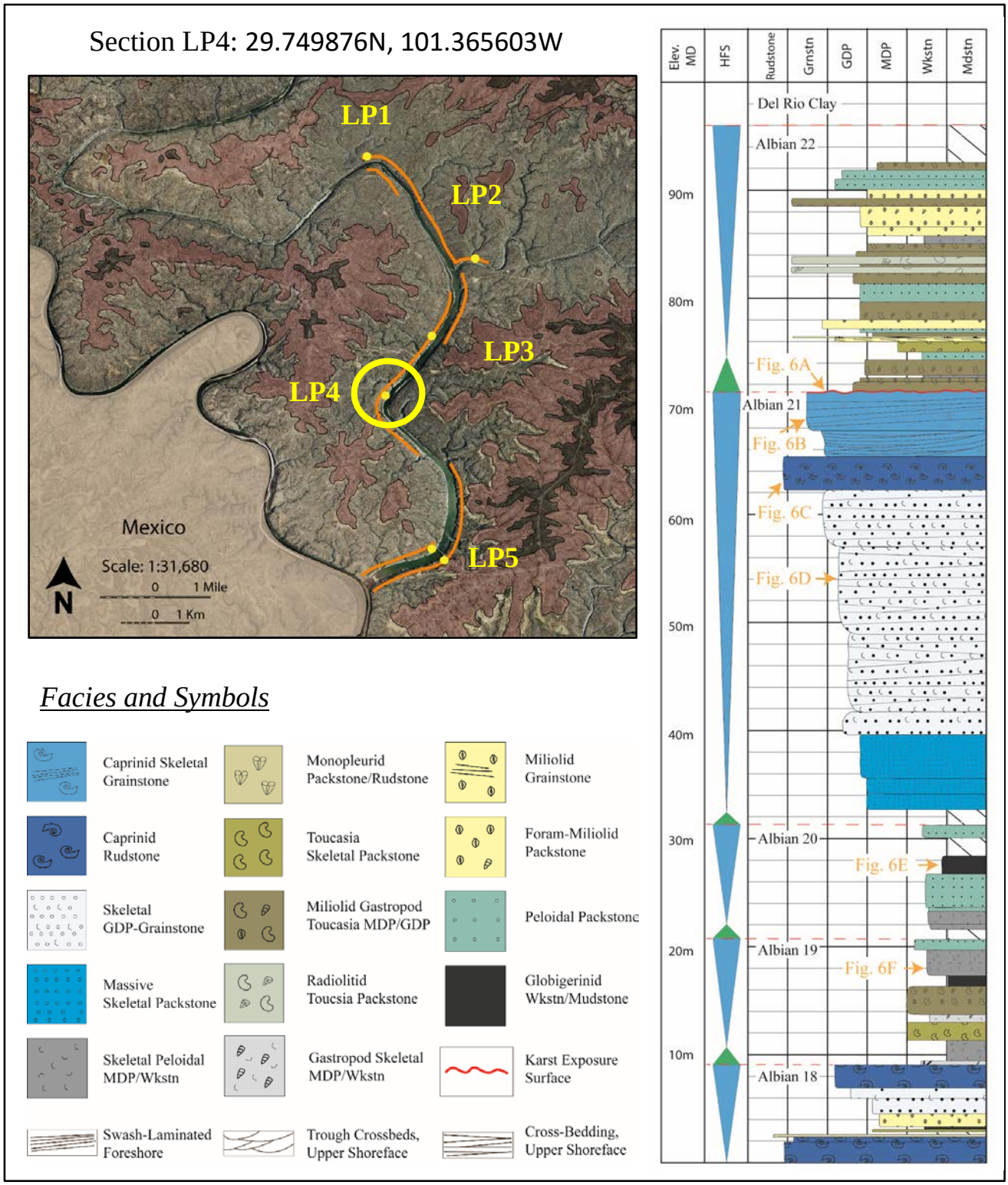

Figure 18: Measured section LP4, ZT Section South of the Railroad Bridge.

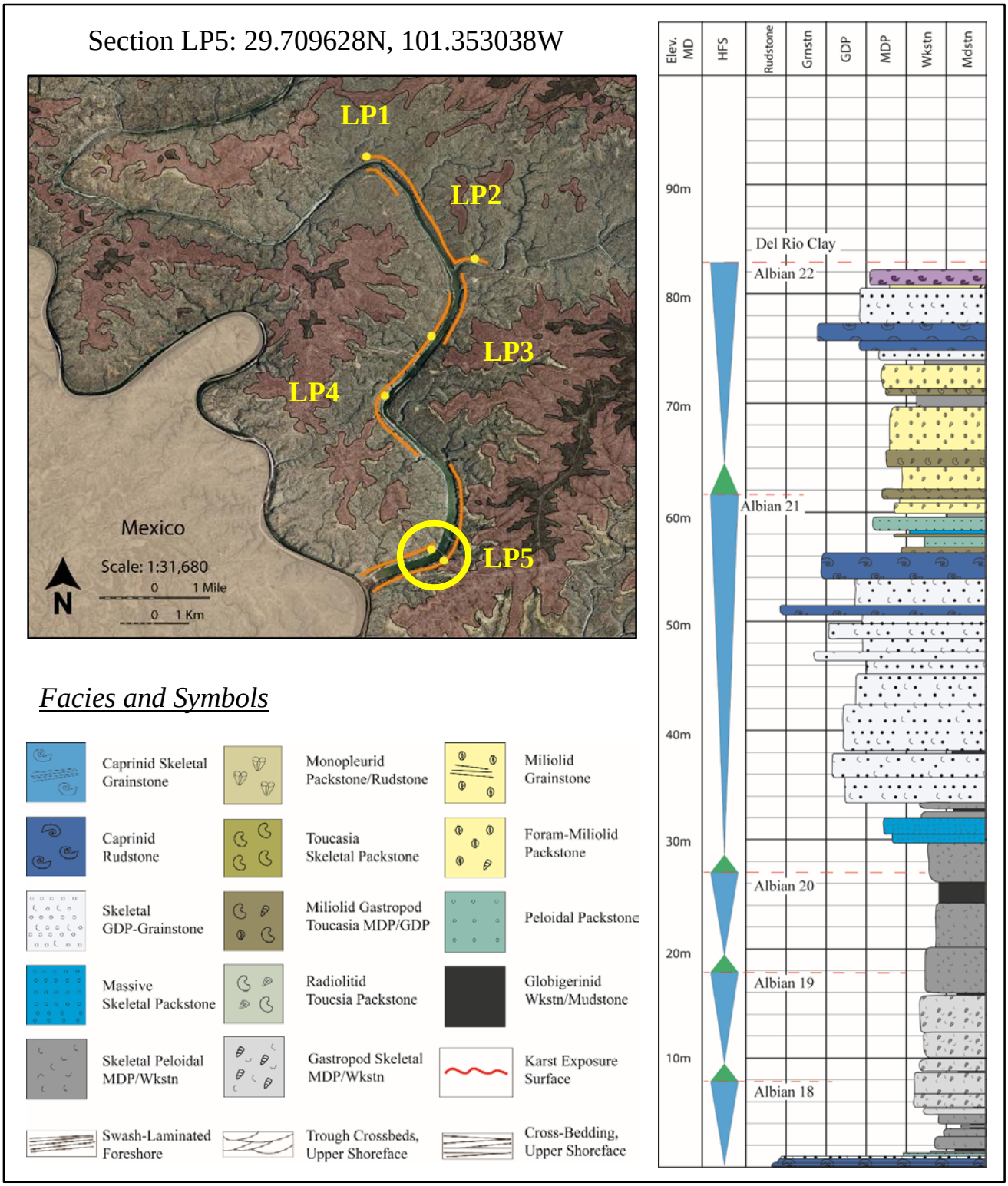

Figure 19: Measured section LP5, Highway 90 Bridge.

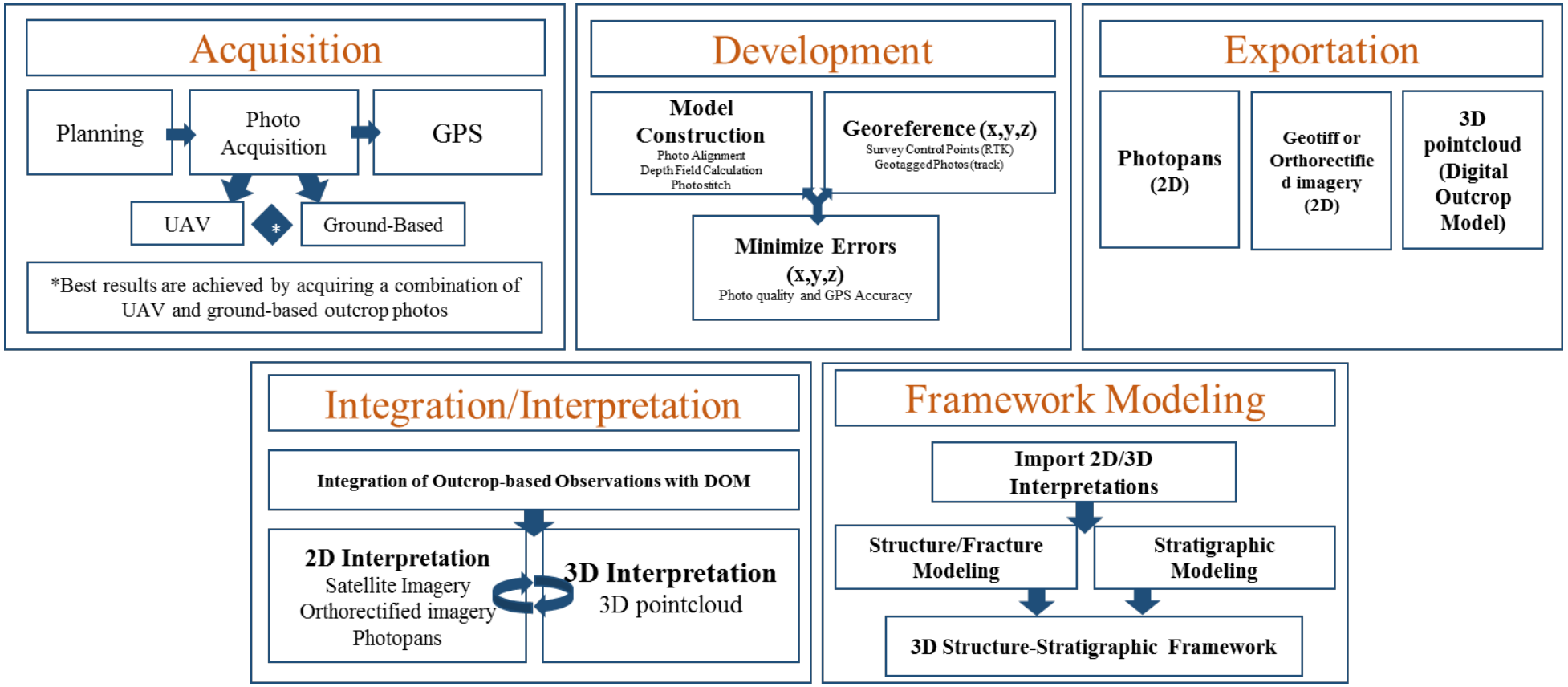

Figure 20: Workflow for construction of 3D digital outcrop models using photogrametry. Modified from Zahm and Kerans, (2014).

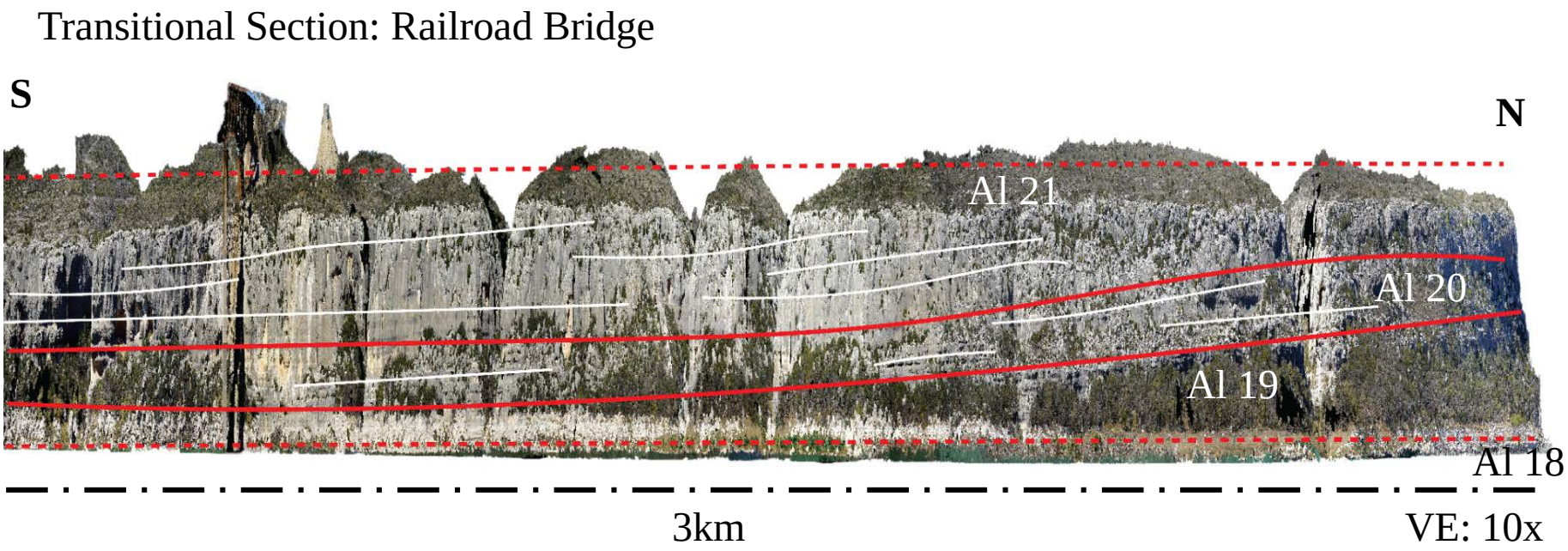

Figure 21: Interpretation of the HFS surface boundaries at the Railroad Bridge using a vertically streched pointcloud.

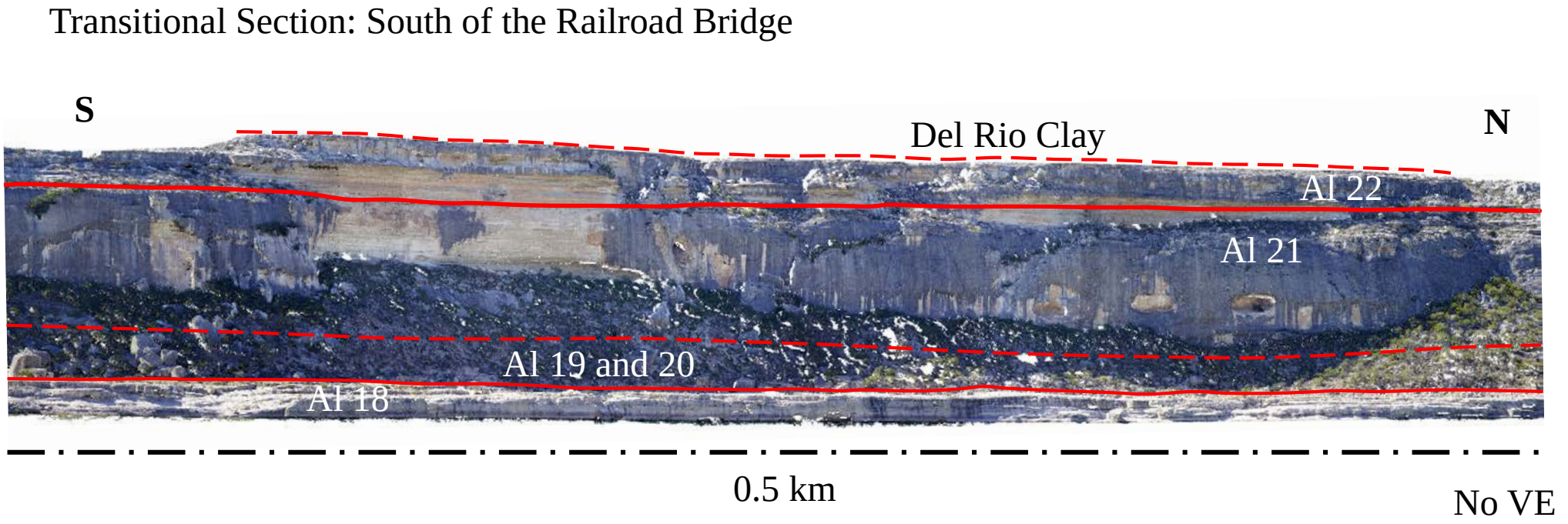

Figure 22: Interpretation of the HFS surface boundaries south of the Railroad Bridge using a dense pointcloud.

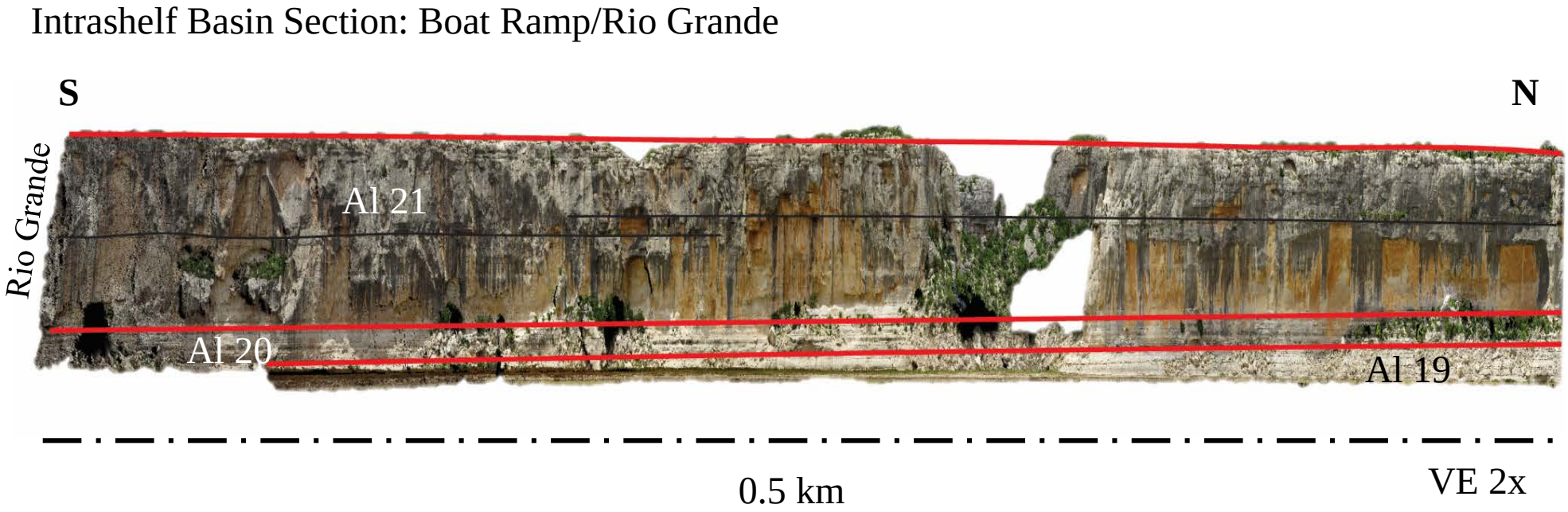

Figure 23: Interpretation of the HFS surface boundaries south of the Highway 90 Bridge using a streched pointcloud.

A) Albian 21 High-frequency Sequence

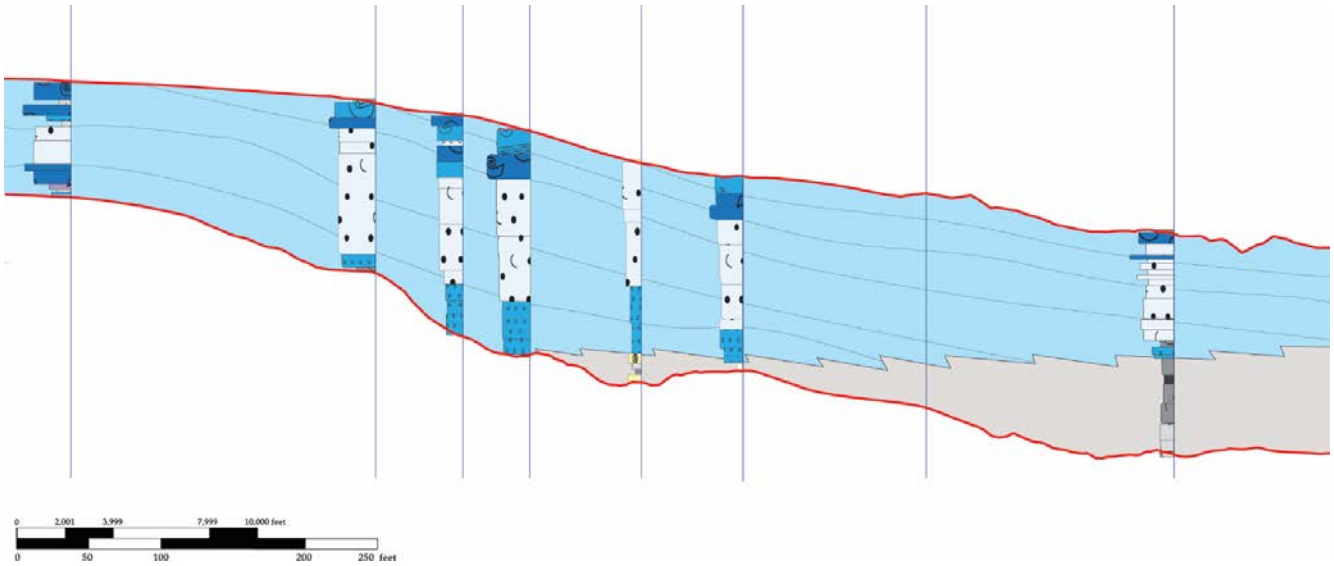

B) Albian 20 High-frequency Sequence

C) Albian 19 High-frequency Sequence

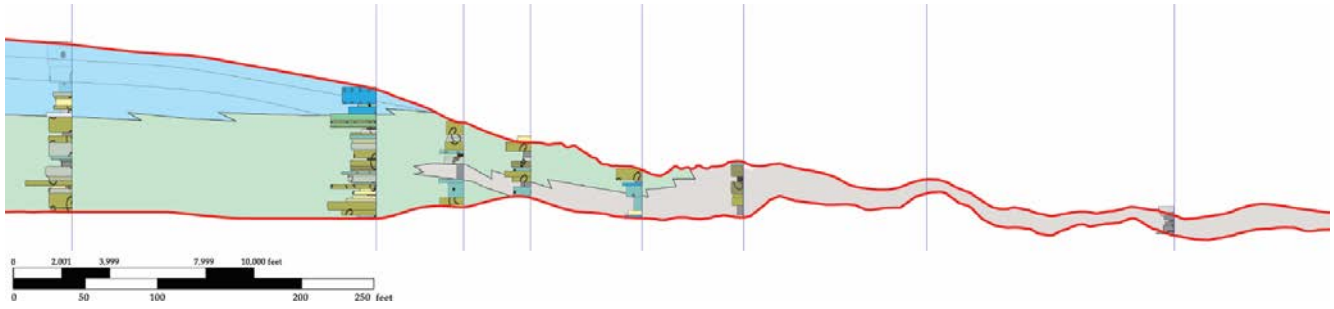

Figure 24: Comparison of the Albian 19-21 high-frequency sequences.

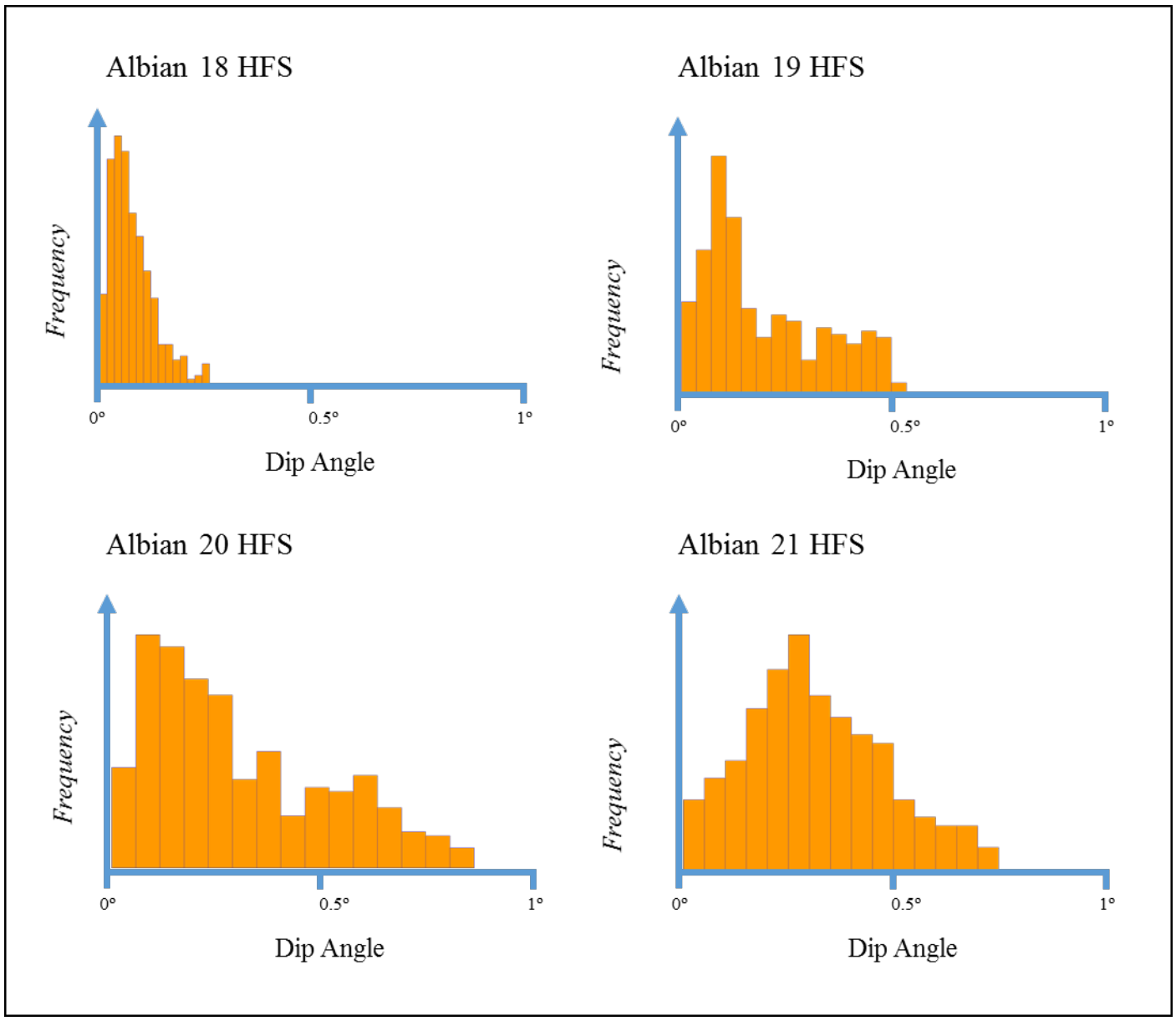

Figure 25: Histogram of the Dip-angle across the depositional profile for the Albian 18-21HFS. Note the bimodal distribution shown in the Albian 19 and 20 HFS marks the transition from the shelf to ISB.

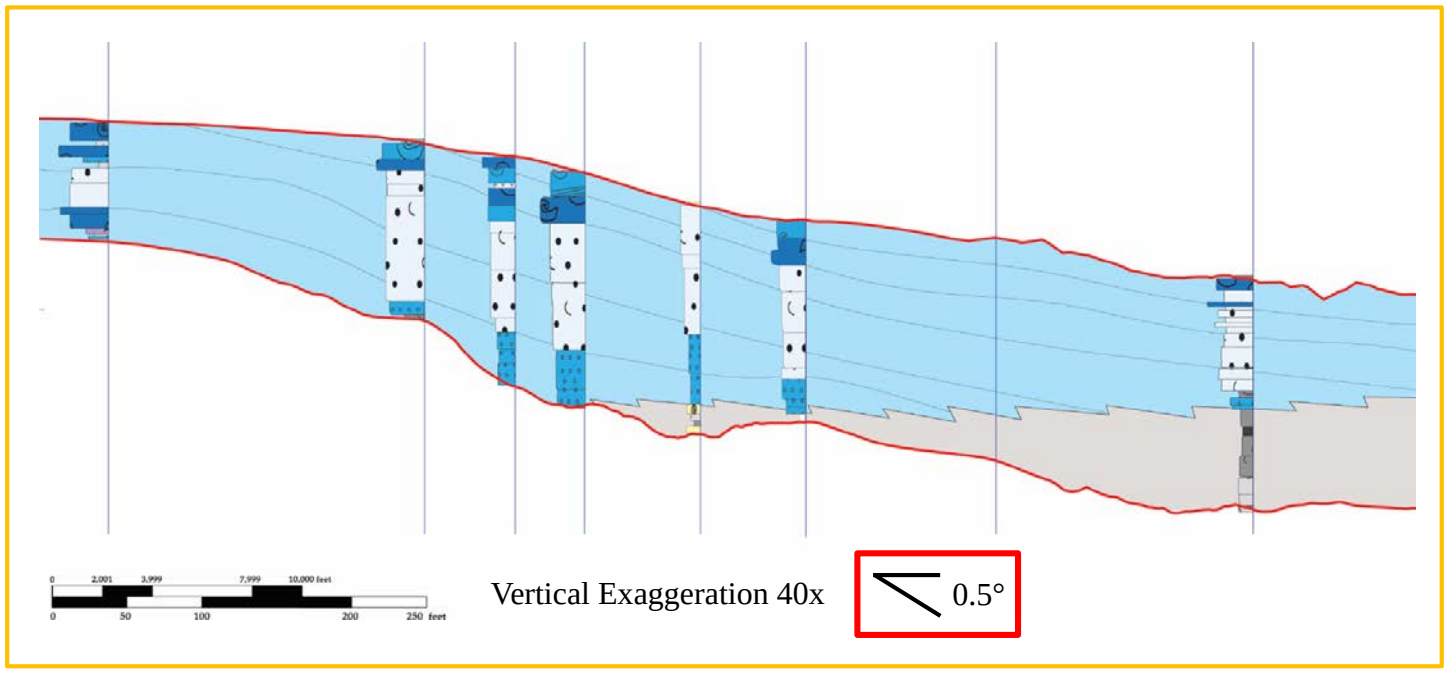

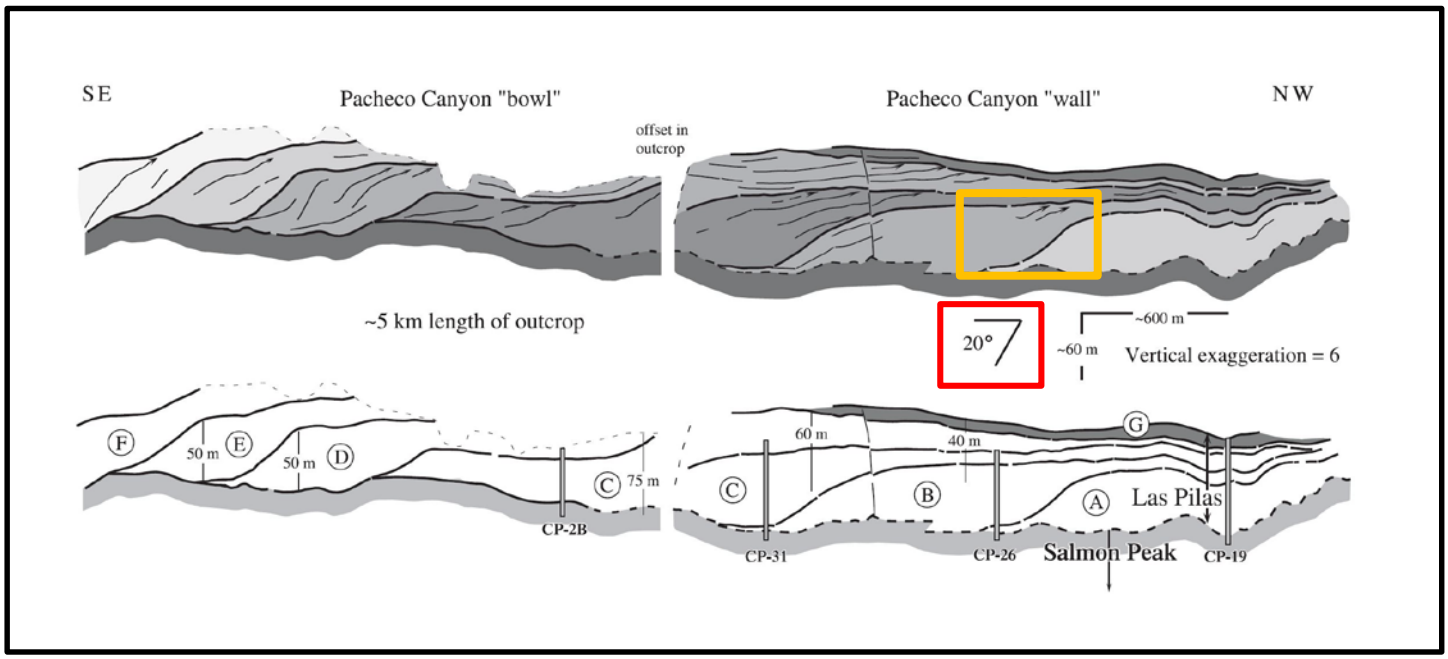

Figure 26: Comparison of the Albian 21 HFS from the northern margin of the Maverick ISB in the top figure, and the western margin below. Osleger, (2004).

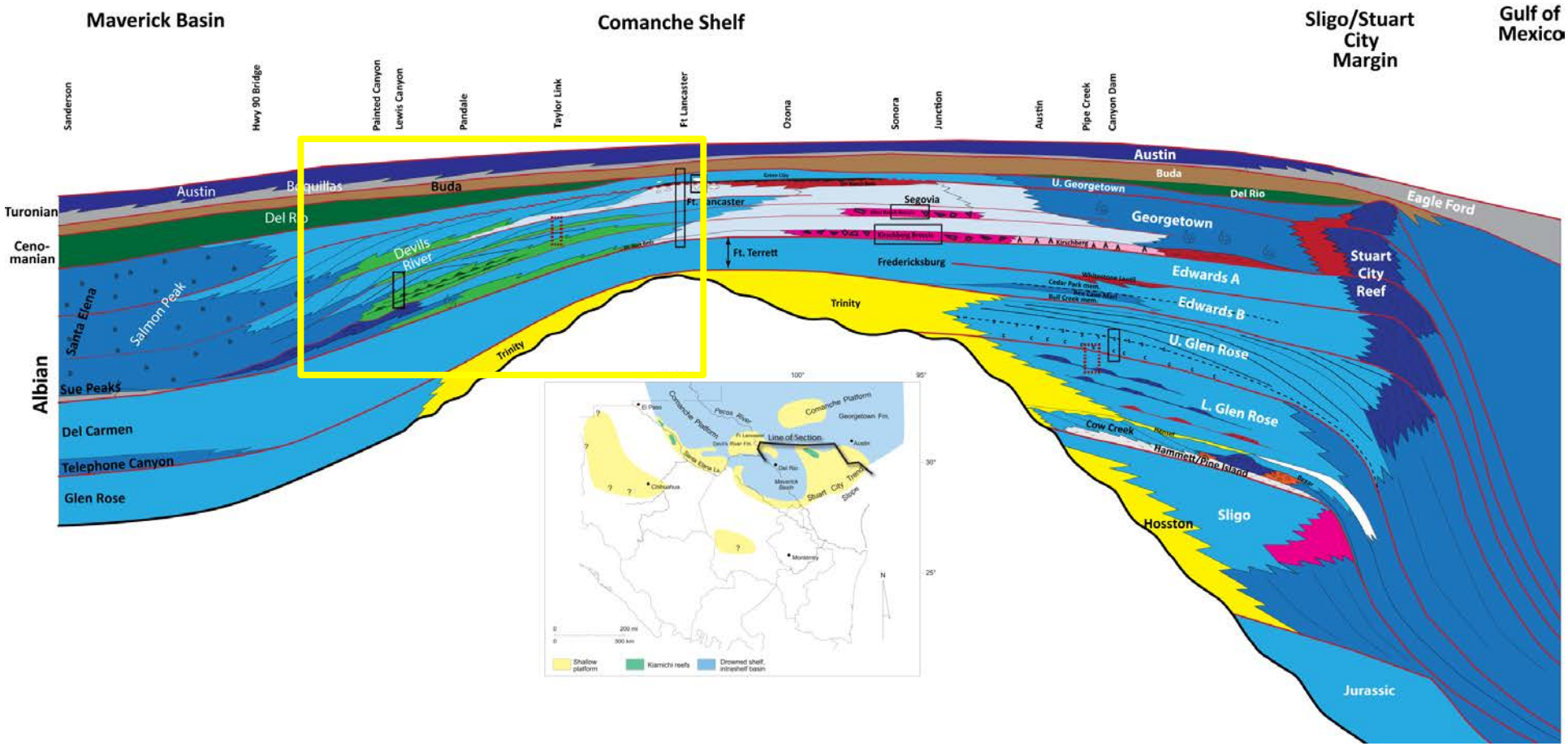

Figure 27: Regional Cretaceous Cross section across the Comanche Shelf. Note the Maverick ISB and the Devils River-Salmon Peak Formation on the left side of the figure. The margin of the Late Albian Maverick ISB is denoted by the yellow box. Figure from Kerans, (2010).

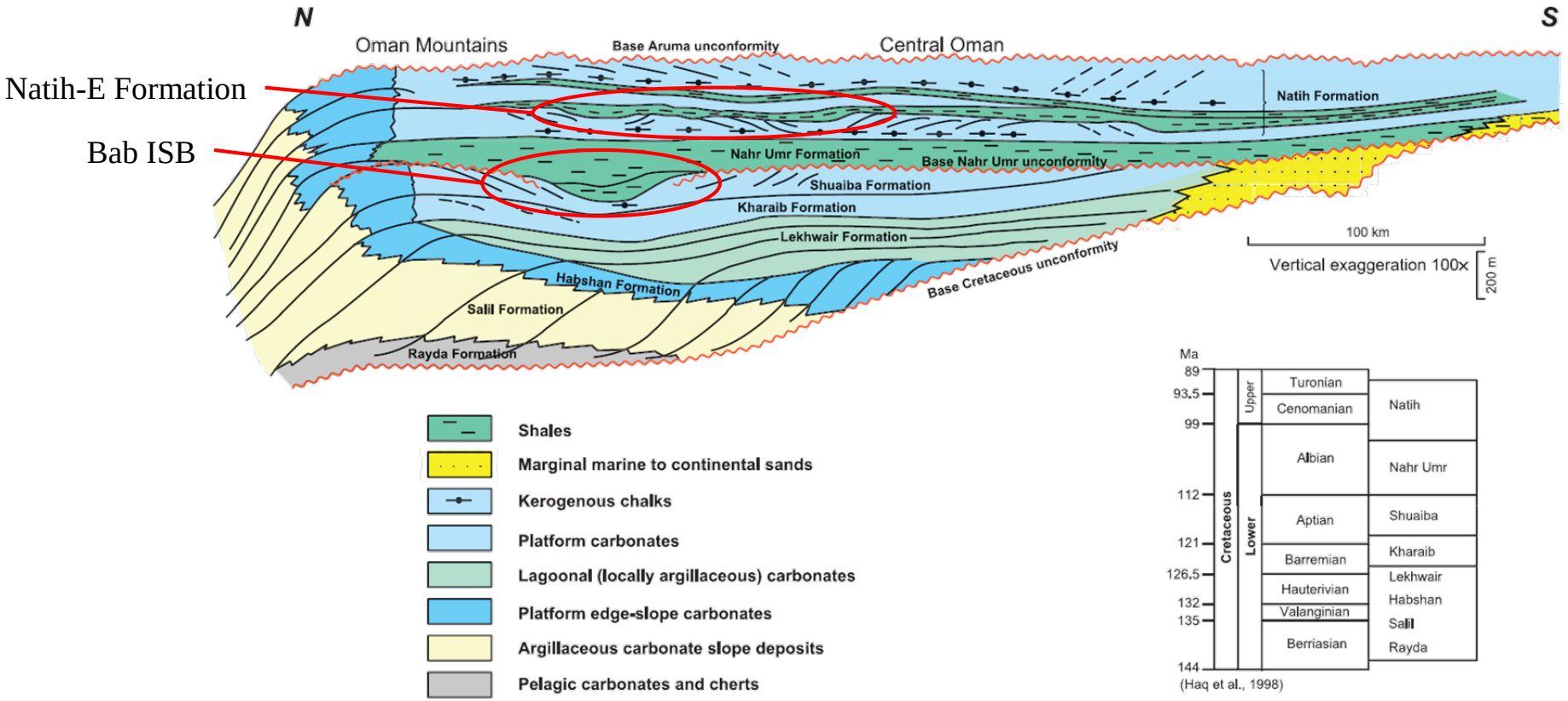

Figure 28: Regional cross section through Oman. This section highlights the Bab Intrashelf Basin (Shuaiba Formaiton) and the Natih-E Formation location behind the protected Habshan Shelf-edge. The constructional developed ISBs are circled in red.

NW Natih-E Formation, Van Buchem et al., (2001) SE

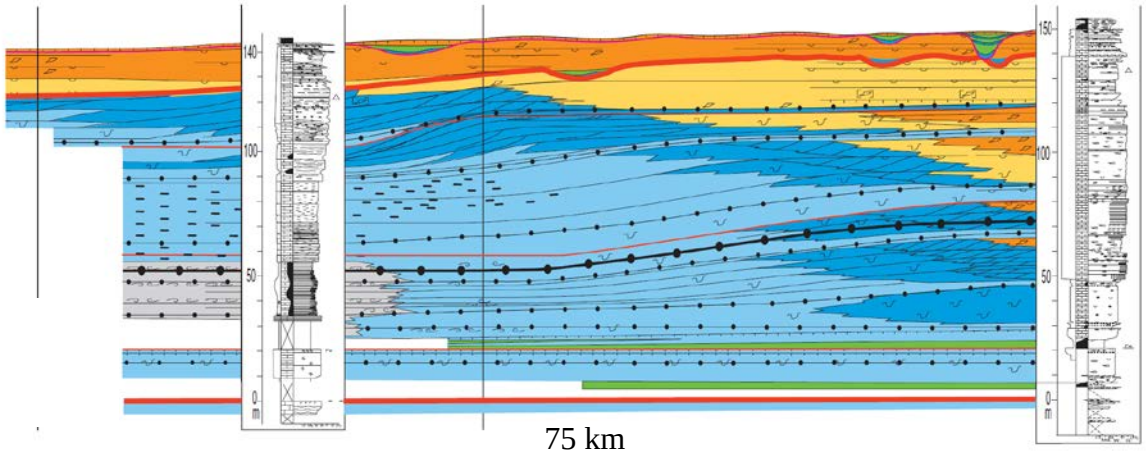

75 km

S Shuaiba Fm. Bab ISB, Yose et al., (2006) N

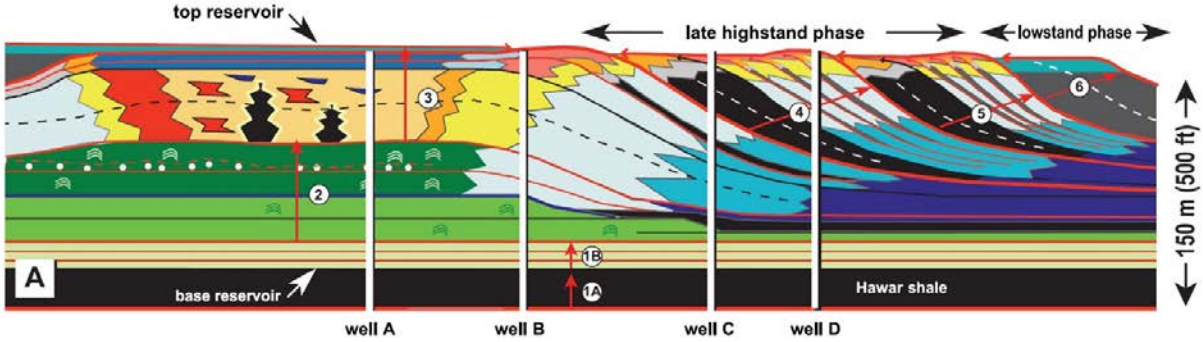

50 km

N Devils River Fm. Maverick ISB, Kerans, (2002) S

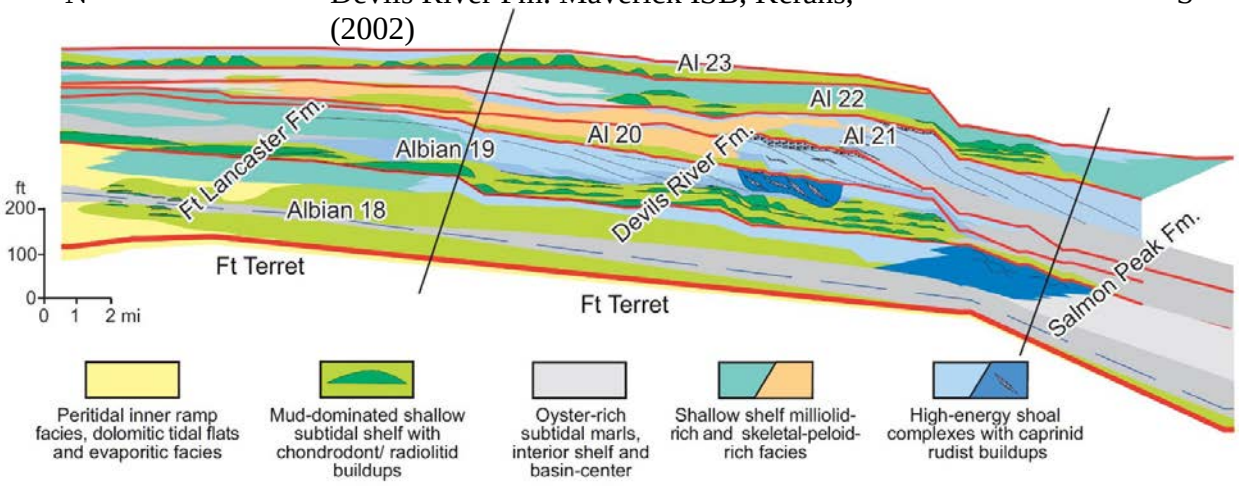

60 km

Figure 29: Comparison of three constructional–accumulation driven ISB systems. Sections from Van Buchem et al., (2002); Yose et al., (2006); Kerans, (2002).

REFERENCES CITED

Alsharhan, A., 1985, Depositional environment, reservoir units evolution, and hydrocarbon habitat of Shuaiba formation, Lower Cretaceous, Abu Dhabi, United Arab Emirates: AAPG Bulletin, v. 69, p. 899-912.

Alsharhan, A., 1995, Facies variation, diagenesis, and exploration potential of the Cretaceous rudist-bearing carbonates of the Arabian Gulf: AAPG bulletin, v. 79, p. 531-550.

Bebout, D. G., and R. G. Loucks, 1974, Stuart City Trend, Lower Cretaceous, South Texas: a carbonate shelf-margin model for hydrocarbon exploration, Univ. of Texas, Austin, TX.

Bellian, J. A., C. Kerans, and D. C. Jennette, 2005, Digital outcrop models: applications of terrestrial scanning lidar technology in stratigraphic modeling: Journal of Sedimentary Research, v. 75, p. 166-176.

Bourget, J., R. Nanson, R. B. Ainsworth, S. Courgeon, S. Jorry, and H. Al-Anzi, 2013, Seismic stratigraphy of a Plio-quaternary Intra-shelf Basin (Bonaparte Shelf, NW Australia): WABS Symposium 2013.

Burchette, T., and V. Wright, 1992, Carbonate ramp depositional systems: Sedimentary Geology, v. 79, p. 3-57.

Burchette, T. P., 1993, Mishrif Formation (Cenomanian-Turonian), Southern Arabian Gulf: Carbonate Platform Growth Along a Cratonic Basin Margin: Chapter 16.

Droste, H., 1990, Depositional cycles and source rock development in an epeiric intra-platform basin: the Hanifa Formation of the Arabian peninsula: Sedimentary Geology, v. 69, p. 281-296.

Droste, H., 2010, High-resolution seismic stratigraphy of the Shu'aiba and Natih formations in the Sultanate of Oman: implications for Cretaceous epeiric carbonate platform systems: Geological Society, London, Special Publications, v. 329, p. 145-162.

Droste, H., and M. Van Steenwinkel, 2004, Stratal geometries and patterns of platform carbonates: the Cretaceous of Oman.

Dunham, R. J., 1962, Classification of carbonate rocks according to depositional textures.

Eliuk, L. S., 1978, The Abenaki Formation, Nova Scotia Shelf, Canada--a depositional and diagenetic model for a Mesozoic carbonate platform: Bulletin of Canadian Petroleum Geology, v. 26, p. 424-514.

Goldhammer, R., 1991, Sequence Stratigraphy and Cyclostratigraphy of the Mesozoic of the Sierra Madre Oriental, Northeast Mexico: A Field Guidebook.

Goldhammer, R., and C. Johnson, 1999, Mesozoic sequence stratigraphy and paleogeographic evolution of northeast Mexico: SPECIAL PAPERS-GEOLOGICAL SOCIETY OF AMERICA, p. 1-58.

Handford, C. R., and R. G. Loucks, 1993, Carbonate depositional sequences and systems tracts-responses of carbonate platforms to relative sea-level changes: MEMOIRS-AMERICAN ASSOCIATION OF PETROLEUM GEOLOGISTS, p. 3-3.

Howell, J. A., A. W. Martinius, and T. R. Good, 2014, The application of outcrop analogues in geological modelling: a review, present status and future outlook: Geological Society, London, Special Publications, v. 387, p. 1-25.

Jackson, M., and S. Seni, 1983, Geometry and evolution of salt structures in a marginal rift basin of the Gulf of Mexico, east Texas: Geology, v. 11, p. 131-135.

Kerans, C., 2002, Styles of rudist buildup development along the northern margin of the Maverick Basin, Pecos River Canyon, southwest Texas.

Kerans, C., 2007, Cretaceous Reservoir Heterogeneity Styles: Facies to Fractures: Reservoir Characterization Research Labratory Annual Field Trip: The Univeristy of Texas at Austin, Bureau of Economic Geology, Field Trip Guidebook.

Kerans, C., W. Fitchen, L. Zahm, and K. Kempter, 1995, High-frequency sequence framework of Cretaceous (Albian) carbonate ramp reservoir analog outcrops: Pecos River Canyon, northwestern Gulf of Mexico Basin: The University of Texas at Austin, Bureau of Economic Geology, Field Trip Guidebook.

Kerans, C., and W. M. Fitchen, 1995, Sequence hierarchy and facies architecture of a carbonate-ramp system: San Andres Formation of Algerita Escarpment and western Guadalupe Mountains, west Texas and New Mexico, v. 235, Bureau of Economic Geology, University of Texas at Austin.

Kerans, C., F. J. Lucia, and R. Senger, 1994, Integrated characterization of carbonate ramp reservoirs using Permian San Andres Formation outcrop analogs: AAPG bulletin, v. 78, p. 181-216.

Kerans, C., and S. W. Tinker, 1997, Sequence stratigraphy and characterization of carbonate reservoirs.

Lehmann, C., D. A. Osleger, and I. Montañez, 2000, Sequence stratigraphy of Lower Cretaceous (Barremian-Albian) carbonate platforms of northeastern Mexico: Regional and global correlations: Journal of Sedimentary Research, v. 70, p. 373-391.

Lehmann, C., D. A. Osleger, and I. P. Montanez, 1998, Controls on cyclostratigraphy of Lower Cretaceous carbonates and evaporites, Cupido and Coahuila platforms, northeastern Mexico: Journal of Sedimentary Research, v. 68.

Lozo, F., and C. Smith, 1964, Revision of Comanche Cretaceous stratigraphic nomenclature, southern Edwards Plateau, southwest Texas.

Markello, J., and J. Read, 1981, Carbonate ramp-to-deeper shale shelf transitions of an Upper Cambrian intrashelf basin, Nolichucky Formation, Southwest Virginia Appalachians: Sedimentology, v. 28, p. 573-597.

Meyer, K. M., and L. R. Kump, 2008, Oceanic euxinia in Earth history: causes and consequences: Annu. Rev. Earth Planet. Sci., v. 36, p. 251-288.

Mitchum, R. M., and J. C. Van Wagoner, 1991, High-frequency sequences and their stacking patterns: sequence-stratigraphic evidence of high-frequency eustatic cycles: Sedimentary Geology, v. 70, p. 131-160.

Murris, R., 1984, Middle East: stratigraphic evolution and oil habitat.

Osleger, D. A., R. Barnaby, and C. Kerans, 2004, A Laterally accreting grainstone margin from the Albian of northern Mexico: Outcrop model for Cretaceous carbonate reservoirs.

Phelps, R. M., C. Kerans, R. O. Da-Gama, J. Jeremiah, D. Hull, and R. G. Loucks, 2015, Response and recovery of the Comanche carbonate platform surrounding multiple Cretaceous oceanic anoxic events, northern Gulf of Mexico: Cretaceous Research, v. 54, p. 117-144.

Phelps, R. M., C. Kerans, R. G. Loucks, R. O. Da Gama, J. Jeremiah, and D. Hull, 2014, Oceanographic and eustatic control of carbonate platform evolution and sequence stratigraphy on the Cretaceous (Valanginian–Campanian) passive margin, northern Gulf of Mexico: Sedimentology, v. 61, p. 461-496.

Pringle, J., J. Howell, D. Hodgetts, A. Westerman, and D. Hodgson, 2006, Virtual outcrop models of petroleum reservoir analogues: a review of the current state-of-the-art: First break, v. 24.

Pringle, J., A. Westerman, J. Clark, N. Drinkwater, and A. Gardiner, 2004, 3D high-resolution digital models of outcrop analogue study sites to constrain reservoir model uncertainty: an example from Alport Castles, Derbyshire, UK: Petroleum Geoscience, v. 10, p. 343-352.

Razin, P., F. Taati, and F. Van Buchem, 2010, Sequence stratigraphy of Cenomanian–Turonian carbonate platform margins (Sarvak Formation) in the High Zagros, SW Iran: an outcrop reference model for the Arabian Plate: Geological Society, London, Special Publications, v. 329, p. 187-218.

Read, J. F., 1985, Carbonate platform facies models: AAPG bulletin, v. 69, p. 1-21.

Read, J. F., 1998, Phanerozoic carbonate ramps from greenhouse, transitional and ice-house worlds: clues from field and modelling studies: Geological Society, London, Special Publications, v. 149, p. 107-135.

Rose, P. R., 1974, Edwards Group, surface and subsurface, central Texas.

Salvador, A., 1991, Origin and development of the Gulf of Mexico basin: The gulf of Mexico basin, p. 389-444.

Scott, R., and C. Kerans, 2004, Late Albian carbonate platform chronostratigraphy, Devils River Formation cycles, west Texas: COURIER-FORSCHUNGSINSTITUT SENCKENBERG., p. 129-148.

Scott, R. W., 1990, Models and stratigraphy of mid-Cretaceous reef communities, Gulf of Mexico.

Smith, C. I., 1981, Review of the geologic setting, stratigraphy, and facies distribution of the Lower Cretaceous in northern Mexico: Lower Cretaceous stratigraphy and structure, northern Mexico: West Texas Geological Society Publication, p. 81-74.

Smith, C. I., J. B. Brown, and F. E. Lozo, 2000, Regional Stratigraphic Cross Sections, Comanche Cretaceous (Fredericksburg-Washita Division), Edwards and Stockton Plateaus, West Texas: Interpretation of Sedimentary Facies, Depositional Cycles, and Tectonics, Bureau of Economic Geology, University of Texas at Austin.

Sonnenfeld, M. D., and T. A. Cross, 1993, Volumetric Partitioning and Facies Differentiation within the Permian Upper San Andres Formation of Last Chance Canyon, Guadalupe Mountains, New Mexico: Chapter 17.

Strecha, C., R. Zoller, S. Rutishauser, B. Brot, K. Schneider-Zapp, V. Chovancova, M. Krull, and L. Glassey, 2015, TERRESTRIAL 3D MAPPING USING FISHEYE AND PERSPECTIVE SENSORS.

Vail, P. R., 1987, Seismic stratigraphy interpretation using sequence stratigraphy: Part 1: Seismic stratigraphy interpretation procedure.

Van Buchem, F., B. Pittet, H. Hillgarten, J. Grotsch, A. Al-Mansouri, I. Billing, H. Droste, H. Oterdoom, and M. Van Steenwinkel, 2002a, High-resolution sequence stratigraphic architecture of the Barremian-Aptian carbonate systems in northern Oman and the United Arab Emirates Kharaib and Shu'aiba Formations: GEOARABIA-MANAMA-, v. 7, p. 461-500.

Van Buchem, F. S., P. Razin, P. W. Homewood, W. H. Oterdoom, and J. Philip, 2002b, Stratigraphic organization of carbonate ramps and organic-rich intrashelf basins: Natih Formation (middle Cretaceous) of northern Oman: AAPG bulletin, v. 86, p. 21-53.

van Buchem, F. S., P. Razin, P. W. Homewood, J. M. Philip, G. P. Eberli, J.-P. Platel, J. Roger, R. Eschard, G. M. Desaubliaux, and T. Boisseau, 1996, High resolution sequence stratigraphy of the Natih Formation (Cenomanian/Turonian) in Northern Oman: distribution of source rocks and reservoir facies: GeoArabia, v. 1, p. 65-91.

Van Wagoner, J. C., R. Mitchum, K. Campion, and V. Rahmanian, 1990, Siliciclastic sequence stratigraphy in well logs, cores, and outcrops: concepts for high-resolution correlation of time and facies.

Webster, R. E., 1980, Structural Analysis of Devils River Uplift-Southern Val Verde Basin, Southwest Texas: AAPG Bulletin, v. 64, p. 221-241.

Wilson, J. L., 1975, Carbonate facies in geologic history, Springer Science & Business Media.

Winker, C. D., and R. T. Buffler, 1988, Paleogeographic evolution of early deep-water Gulf of Mexico and margins, Jurassic to Middle Cretaceous (Comanchean): AAPG Bulletin, v. 72, p. 318-346.

Yose, L. A., A. S. Ruf, C. J. Strohmenger, J. S. Schuelke, A. Gombos, I. Al-Hosani, S. Al-Maskary, G. Bloch, Y. Al-Mehairi, and I. G. Johnson, 2006, Three-dimensional characterization of a heterogeneous carbonate reservoir, Lower Cretaceous, Abu Dhabi (United Arab Emirates).

Zahm, C. K., and C. Kerans, 2014, Unmanned Aerial Vehicles (UAVs) and Digital Outcrop Models of Carbonate Reservoir Analogs, AAPG Annual Convention and Exhibition.

Zahm, L. C., 1997, Depositional model and sequence stratigraphic framework for upper Albian/lower Cenomanian carbonate ramp, Western Comanche Shelf, Texas.

Ziegler, M. A., 2001, Late Permian to Holocene paleofacies evolution of the Arabian Plate and its hydrocarbon occurrences: GEOARABIA-MANAMA-, v. 6, p. 445-504.

VITA

Jeffrey Robert Sitgreaves was born in Nacogdoches, Texas in 1991. He attended Brackett High School in Brackettville, Texas. It was there, he was first introduced to the geological sciences when he participated in GeoFORCE Texas, a STEM outreach program supported by the Jackson School of Geosciences. It was this program that encouraged him to pursue an education and career in the geosciences at The University of Texas at Austin. He received his Bachelor of Science in the Geological Sciences in 2013. It was during his undergraduate experience that he met his advisor Dr. Charles Kerans, who encouraged and motivated him to pursue a specialty in carbonate sequence stratigraphy and sedimentology. In the Fall of 2013, Jeffrey continued his education at UT Austin when he enrolled to pursue a M.S in the Geological Sciences. During this time, he worked as a research assistant for the Reservoir Characterization Research Laboratory (RCRL), and served as teaching assistant for the undergraduate-level Field Methods course. In January 2016, Jeffrey will begin a career at ExxonMobil in The Woodlands, Texas.

Permanent email: jeffrey.sitgreaves@gmail.com

This thesis was typed by Jeffrey R. Sitgreaves